DRAFT VERSION JUNE 16, 2021
Typeset using LaTeX **twocolumn** style in AASTeX63

Distant Relatives: The Chemical Homogeneity of Comoving Pairs Identified in Gaia

TYLER NELSON,[1] YUAN-SEN TING,[2,3,4,5] KEITH HAWKINS,[1] ALEXANDER JI,[4] HARSHIL KAMDAR,[6] AND KAREEM EL-BADRY[7]

[1]*Department of Astronomy, The University of Texas at Austin, 2515 Speedway Boulevard, Austin, TX 78712, USA*
[2]*Institute for Advanced Study, Princeton, NJ 08540, USA*
[3]*Department of Astrophysical Sciences, Princeton University, Princeton, NJ 08544, USA*
[4]*Observatories of the Carnegie Institution of Washington, 813 Santa Barbara Street, Pasadena, CA 91101, USA*
[5]*Research School of Astronomy & Astrophysics, Australian National University, Cotter Rd., Weston, ACT 2611, Australia*
[6]*Harvard-Smithsonian Center for Astrophysics, Cambridge, MA, 02138, USA*
[7]*Department of Astronomy and Theoretical Astrophysics Center, University of California Berkeley, Berkeley, CA 94720*

(Dated: Accepted XX. Received YY; in original form ZZ)

ABSTRACT

Comoving pairs, even at the separations of $\mathcal{O}(10^6)$ AU, are a predicted reservoir of conatal stars. We present detailed chemical abundances of 62 stars in 31 comoving pairs with separations of $10^2 - 10^7$ AU and 3D velocity differences < 2 km s^{-1}. This sample includes both bound comoving pairs/wide binaries and unbound comoving pairs. Observations were taken using the MIKE spectrograph on the Magellan/Clay Telescope at high resolution (R $\sim 45,000$) with a typical signal-to-noise ratio of 150 per pixel. With these spectra, we measure surface abundances for 24 elements, including Li, C, Na, Mg, Al, Si, Ca, Sc, Ti, V, Cr, Mn, Fe, Co, Ni, Cu, Zn, Sr, Y, Zr, Ba, La, Nd, Eu. Taking iron as the representative element, our sample of wide binaries is chemically homogeneous at the level of 0.05 dex, which agrees with prior studies on wide binaries. Importantly, even systems at separations $2 \times 10^5 - 10^7$ AU are homogeneous to 0.09 dex, as opposed to the random pairs which have a dispersion of 0.23 dex. Assuming a mixture model of the wide binaries and random pairs, we find that $73 \pm 22\%$ of the comoving pairs at separations $2 \times 10^5 - 10^7$ AU are conatal. Our results imply that a much larger parameter space of phase space may be used to find conatal stars, to study M-dwarfs, star cluster evolution, exoplanets, chemical tagging, and beyond.

Keywords: Stars: abundances, Stars: binaries, Stars: kinematics and dynamics, Stars: late-type

1. INTRODUCTION

Stars which are born from the same gas, i.e., conatal, are critical in astronomy. The conatal nature of open clusters and wide binaries have made them indispensable laboratories for testing and improving our understanding of various areas of Galactic and stellar astrophysics. Both open clusters and wide binaries have been used to evaluate the current feasibility of chemical tagging (De Silva et al. 2007; Ting et al. 2012; Ness et al. 2018; Andrews et al. 2019; Hawkins et al. 2020b). Open clusters are used to calibrate stellar parameter and chemical abundance pipelines for large surveys (e.g., García Pérez et al. 2016). Wide binaries can be used to calibrate the metallicity of M-dwarfs (e.g., Lépine & Bongiorno 2007; Rojas-Ayala et al. 2010; Montes et al. 2018), constrain the age-magnetic activity relation (e.g., Garcés et al. 2011; Booth et al. 2017), the age-metallicity relation (e.g., Rebassa-Mansergas et al. 2016), and the initial-final mass relation (e.g., Zhao et al. 2012; Andrews et al. 2015). Besides, we can also use wide binaries to study exoplanet engulfment (e.g., Meléndez et al. 2017; Oh et al. 2018).

Gravitationally bound binaries favor a conatal origin. For separations within a few thousand AU, binaries are mostly formed via turbulent core fragmentation (Offner et al. 2010; Lee et al. 2017). At separations up to $\sim 10^5$ AU, wide binaries can be formed from dynamical unfolding of triple systems (Reipurth & Mikkola 2012), the evaporation of star clusters (Kouwenhoven et al. 2010; Moeckel & Clarke 2011), and chance gravitational capture of prestellar cores (Tokovinin 2017). The predicted conatal nature of wide binaries motivated studies of their chemistry (Andrews et al. 2019; Ramírez et al. 2019; Hawkins et al. 2020b). They have found wide binaries to be chemically homogeneous to

Corresponding author: Tyler Nelson
tyler.nelson@utexas.edu

$\sim 0.02 - 0.1$ dex in Δ[Fe/H][1]. Nonetheless, the studies of chemical homogeneity for binaries remain rather limited ($\mathcal{O}(10)$ pairs) as large surveys often do not observe both stars due to the subsampling, and we have to resort to targeted studies.

Comoving pairs, on the other hand, are even less studied than wide binaries. The investigation of detailed chemistry for comoving pairs remains largely non-existent for separations beyond a few parsecs. Comoving pairs separated by $\gtrsim 10^5$ AU are no longer bound (Jiang & Tremaine 2010). As outlined in Oh et al. (2017), these unbound systems could arise from disrupted/dissolved conatal systems (open clusters, stellar binaries) or unrelated systems (chance alignments, gravitational resonance). Recently, simulations from Kamdar et al. (2019a) argued comoving pairs have a high probability of being conatal provided that their 3D velocity difference (Δv_{3D}) is below 2 km s^{-1} at separations up to $\mathcal{O}(10^6)$ AU. Their simulations predicted that pairs with separations $\sim 10^6$ AU are $\sim 80\%$ conatal. If true, this could dramatically expand the number of systems that could be conatal, which can improve stellar atmospheric models, study exoplanet engulfment, and calibrate surveys, among other applications. With the precise astrometry provided by the recent data release of Gaia (Gaia Collaboration et al. 2018, 2020) sufficient comoving systems can readily be located, and this study is set up to test this proposition – *are comoving stars with large separations conatal?*

A key characteristic of conatal stars is their chemical composition's homogeneity; conatal stars are expected to have similar initial chemical compositions as they are usually formed from well-mixed ISM gas (Feng & Krumholz 2014). Nonetheless, measured surface abundances can be changed by internal processes (atomic diffusion, rotational mixing, dredge-up, gravitational settling, radiative levitation, Schuler et al. 2011; Dotter et al. 2017), model limitations (incomplete laboratory data, NLTE, 3D Ruchti et al. 2013; Heiter et al. 2015; Nissen & Gustafsson 2018; Jofré et al. 2019), and methodological limitations (Jofré et al. 2014, 2019). All these effects could complicate any interpretation of the chemical homogeneity of the two stars.

To distinguish model systematic from astrophysical processes, in this study, we will appeal to differential analysis of stellar twins – i.e., stellar pairs with similar stellar parameters. Differential abundances can remove many of these effects provided the stars are close in stellar parameters because the systematic effects in the star of interest and reference star largely cancel out (see Gray 2008; Nissen & Gustafsson 2018; Jofré et al. 2019).

[1] Some systems have a larger metallicity difference (e.g., Δ[Fe/H] ~ 0.2 dex, Oh et al. 2018)

In this study, we measure abundance differences in 24 elements for 33 comoving pairs with $\Delta v_{3D} < 2$ km s^{-1} and separations between $\sim 10^2 - 10^7$ AU. With access to homogeneous high resolution, high signal-to-noise data, we uniquely positioned to explore the detailed abundances from the wide binaries and the comoving stars and the chemical homogeneity of the two components. In Section 2 we describe the observations. Section 3 details the methods for estimating stellar parameters and abundances. Our results are presented in Section 4, in which we explore the conatal fraction of the comoving pairs. These results are discussed in Section 5 and summarized in Section 6.

2. DATA PROPERTIES

Our target selection focused on comoving pairs of FG dwarfs within 300 pc of the Solar neighborhood. FG dwarfs were selected because they are both luminous, and their spectral models are best characterized. We create the initial list of sources with the following ADQL query:

```
SELECT *
FROM gaiadr2.gaia_source
WHERE ra > 165
OR ra < 15
AND dec < 25
AND bp_rp BETWEEN 0.5 AND 1.5
AND 1000/parallax < 300
AND parallax_over_error > 5
AND phot_g_mean_mag IS NOT NULL
AND ((phot_g_mean_mag -
    5*LOG10(1000/parallax) + 5) BETWEEN 2
    AND 7)
AND radial_velocity IS NOT NULL
```

Our range of bp_rp was selected to exclude hot stars as some of them could be rapid rotators with broad spectral features which complicate spectral analysis. Next, to ensure that our systems are genuine (isolated) comoving stars, we filter out members of open clusters and stellar associations with a friend-of-friend (FoF) connectivity cut following Kamdar et al. (2021), removing any pairs that belong to an aggregate with more than 4 FoF companions (with separations < 10 pc, $\Delta v_{3D} < 5$ km s^{-1}). We verify the efficacy of this filtering by cross-matching our sample with the open clusters and comoving groups catalogs from Kounkel & Covey (2019) and Cantat-Gaudin & Anders (2020), finding no overlap. From this list of possible sources, we calculate the 3D velocity separation Δv_{3D} and spatial separation using Galpy (Bovy 2015) using astrometry and radial velocities measurements from Gaia DR2. The target selection prioritized stars in similar locations on the color-magnitude diagram (CMD) to reduce the influence of systematic errors on the derived elemental abundances. Together, we consider the comoving pairs that satisfy the following criteria:

- $|\Delta M_G| < 0.5$ mag
- $|\Delta(G_{BP} - G_{RP})| < 0.1$ mag
- $\Delta v_{3D} < 2$ km s^{-1}
- 3D separation < 300 pc

The remaining comoving pairs were binned in log separation and sorted by apparent magnitude. The final sample was selected by taking the most luminous ~ 10 pairs from each log separation bin.

Throughout this study, we will use the term comoving stars to signify both bound and unbound pairs of stellar companions. In particular, for consistency, we will use the words "close" comoving pairs and wide binaries interchangeably to refer to (mostly bound) wide binaries and "far" comoving pairs to be the primarily unbound systems. For simplicity, we define close comoving pairs as those with 3D spatial separation of 1 pc (i.e., 2×10^5 AU), and the others far comoving pairs. This choice is partly motivated by the fact that in simulations from Kamdar et al. (2019b), the minimum separation of unbound comoving pairs have a separation of 1 pc. This is also consistent with the previous study from Jiang & Tremaine (2010).

We observed 33 pairs of comoving stars using the MIKE spectrograph on the *Magellan/Clay* telescope (Bernstein et al. 2003) from June 13 to June 16, 2019. These 33 pairs constitute our "main sample". We also observe two additional pairs with $\Delta v_{3D} > 2$ km s^{-1} as a control sample. But unless otherwise stated, we will only refer to the main sample throughout this study. Additionally, we also observed four Gaia benchmark stars (Jofré et al. 2014; Blanco-Cuaresma et al. 2014b; Heiter et al. 2015) dispersed over the sampled CMD to improve the data reduction. The benchmark stars used were 18 Sco, bet Vir, HD 140283, and mu Ara. The instrument employs a blue and red spectrograph to cover 3350–5000 Å and 4900–9500 Å respectively. We used the 0.5" slit with 2×1 binning, which gave the blue and red spectrographs typical resolving powers of 50,000 and 40,000, respectively. The median signal-to-noise ratio (SNR) per pixel for the blue and red chips were 121 and 185. The observational details are given in Table 1.

Our sample size of 33 pairs is comparable to previous detailed chemical studies of wide binaries (Andrews et al. 2019; Ramírez et al. 2019; Hawkins et al. 2020b), but expands the range of separations by two orders of magnitude. Previous studies mostly restrict their sample to $\lesssim 10^5$ AU, whereas in this study we have comoving pairs with separations up to 10^7 AU. In the top panel of Figure 1 we show the CMD of our comoving targets (white circles) with a random sample of 200,000 stars from Gaia DR2 plotted in the background for reference.

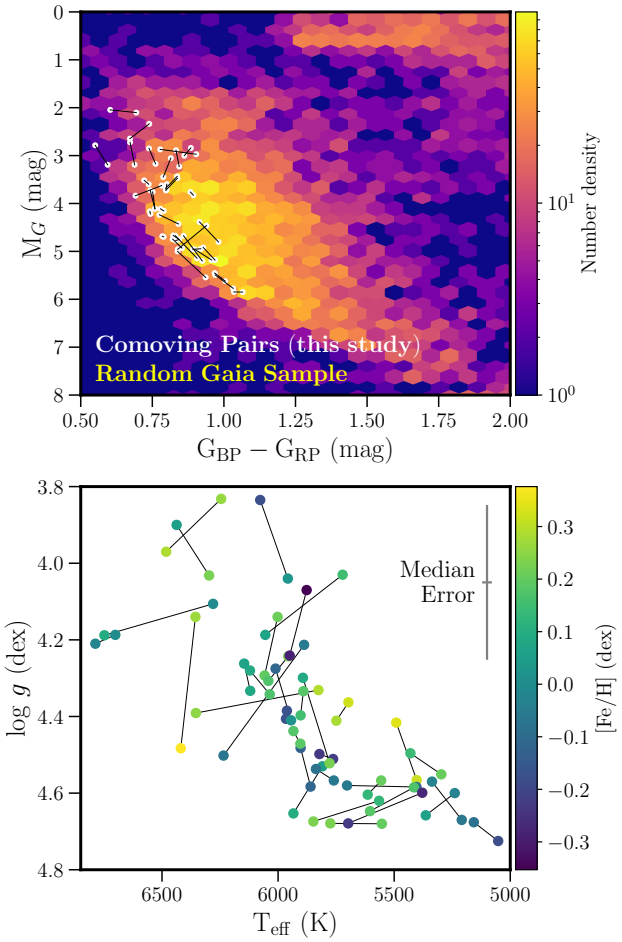

Figure 1. Top panel: The observed stars (white circles) are overplotted on 200,000 random stars from Gaia DR2 (background). Most of the samples are main-sequence stars because giant-giant stellar twins are rare, and we focus on the bright local sample. Bottom panel: Stellar parameter fits for the comoving pairs from BACCHUS. Representative (median) error bars are given in the upper right corner of the plot. For each pair, the two comoving components are connected by a black line.

Among our sample, we found that, for two particular pairs, each of which had a component that exhibit large deviations in the radial velocity measurements from Gaia eDR3[2] and our RV derived with the MIKE spectra. Both systems were flagged as outliers based on the interquartile range (IQR) test[3]. This deviation could indicate an unresolved companion star. We exclude them from the primary sample because the unresolved binaries in hierarchical triplets can bias metal-

[2] Note that the radial velocity in eDR3 follows the one from DR2

[3] Consider a data distribution, with P_i denoting the ith percentile of said distribution. A data point D is labeled an outlier if D is outside the interval $P_{50} \pm 1.5 \times (P_{75} - P_{25})$, where $(P_{75} - P_{25})$ is the interquartile range.

Table 1. Abbreviated target list for the 33 comoving pairs investigated in this study. A complete machine-readable version is available online. For compactness, we only display a subset of the columns. Comoving pairs can be determined using the identifier column. The fourth and fifth columns are the parallax and parallax errors from Gaia eDR3.

Gaia eDR3 ID	Identifier	RA (^{o})	DEC (^{o})	ϖ (mas)	σ_ϖ (mas)	G (mag)	BP - RP (mag)	RV ($\mathrm{km\ s^{-1}}$)	σ_{RV} ($\mathrm{km\ s^{-1}}$)	$\mathrm{SNR_{Blue}}$	... ...
6160638833832941312	CM00A	191.8605	-30.8986	9.931	0.017	4.75	0.84	-12.50	0.05	86	...
3471119180522314624	CM00B	189.8021	-29.1721	9.613	0.014	4.77	0.83	-11.23	0.06	75	...
3613454637229633664	CM01A	206.5261	-11.7535	4.092	0.015	3.45	0.79	22.96	0.03	93	...
3613454637229634176	CM01B	206.5178	-11.7507	4.085	0.016	3.05	0.81	22.17	0.03	120	...
3639520621950395904	CM02A	215.6611	-7.7688	23.742	0.025	4.16	0.74	-32.62	0.03	209	...
3639520621950395776	CM02B	215.6613	-7.7704	23.802	0.024	4.22	0.74	-33.26	0.03	167	...
5897704951769034368	CM03A	218.3675	-52.5846	5.880	0.017	3.47	0.84	43.98	0.03	114	...
5897785667103983616	CM03B	217.2034	-52.9914	5.645	0.018	3.71	0.80	44.24	0.03	94	...
6224633983987510528	CM04A	225.8985	-27.8432	19.433	0.027	4.70	0.79	-15.77	0.03	131	...
6224633983987511552	CM04B	225.9000	-27.8416	19.413	0.029	4.68	0.78	-14.99	0.03	145	...

licity estimates by 0.1 dex (El-Badry et al. 2018). Excluding these pairs leaves us with 31 pairs of comoving stars.

We reduce the raw MIKE data with CarPy (Kelson 2003) which outputs wavelength-calibrated multi-order echelle spectra for the science targets and flats. After flat-fielding, the spectra were normalized by fitting a cubic spline as a pseudo continuum for each order. We determine the pseudo continuum by iterative sigma clipping. We discard 100 pixels on both ends of each order because the blaze function is less well defined due to the lack of signal. Orders are then combined using a flux error weighted average. The sigma clipping process was tuned by comparing observations of four Gaia Benchmark stars to the online library (Blanco-Cuaresma et al. 2014b). We employ iSpec (Blanco-Cuaresma et al. 2014a) to determine the radial velocity (RV) correction and remove cosmic rays.

The reduced spectra for two comoving pairs in the wavelength regime of $5384 \leq \lambda \leq 5400$ Å are shown in Figure 2. In the top panel, we compare the spectra of both components for the two comoving pairs. The bottom panel shows the difference in spectra between the comoving components. Since we only target stellar twins, the difference predominantly comes from the difference in elemental abundances. The two spectra exhibit only minimal differences when they have similar chemistry. The careful selection of stellar twins allows us to derive elemental abundances with high fidelity for this homogeneous sample of comoving pairs.

2.1. *Positions and Velocities*

We calculate the positions and velocities for each star using Gaia eDR3 astrometry and spectroscopic RVs from our observations. Note that we made the target selection with DR2 before eDR3 became available. However, since Gaia eDR3 improves Gaia DR2 astrometry, we decide to use eDR3 astrometry for the final determination and plots throughout this study. This update causes some objects within our main sample to appear outside the $\Delta \mathrm{v_{3D}} < 2\ \mathrm{km\ s^{-1}}$ cut, even though our our main sample are selected to be within this boundary with the DR2 values.

We will consider two approaches to calculate the 3D separations between members of comoving pairs. The first ("method 1") uses the 6D phase space information to calculate the 3D separation directly using a Monte Carlo approach. We construct a multivariate normal distribution for each star with mean of the reported values and a covariance matrix using the 5D measured correlations in astrometry from Gaia eDR3 as well as the RV errors from the iSpec RV fit. We sample from this distribution 10,000 times and apply a transformation from equatorial to Galactic Cartesian coordinates to each sample. Finally, we calculate the 3D separation and velocity difference of the samples in Cartesian coordinates, taking the mean and standard deviation across samples as the point estimate and uncertainty for these quantities.

This method does not invoke additional assumptions about the geometry or separation distribution of pairs. However, for comoving pairs with 3D separations, $\lesssim 10^5$ AU, the uncertainty in 3D separation is often significantly inflated by parallax uncertainties, making it impossible to accurately measure 3D separations using method 1. Consider two stars with identical true parallax, ϖ, and parallax uncertainty, σ_ϖ. In the limit of $\sigma_\varpi/\varpi \ll 1$, the typical difference in *apparent* line-of-sight distance between the two stars is $\Delta d_{\mathrm{apparent}} \sim \frac{1000\,\mathrm{pc}}{(\varpi/\mathrm{mas})} \times \sigma_\varpi/\varpi$. For typical pairs in our sample, with $\varpi \sim 10$ mas and $\sigma_\varpi \sim 0.02$ mas, this translates to an apparent distance difference of $\sim 4 \times 10^4$ AU, which represents the amount by which the distance differences of typical pairs will be inflated by parallax uncertainties. For the pairs in our sample with the smallest ϖ and largest σ_ϖ, this value is $\sim 3 \times 10^5$ AU. This intuition also prompted us to divide the

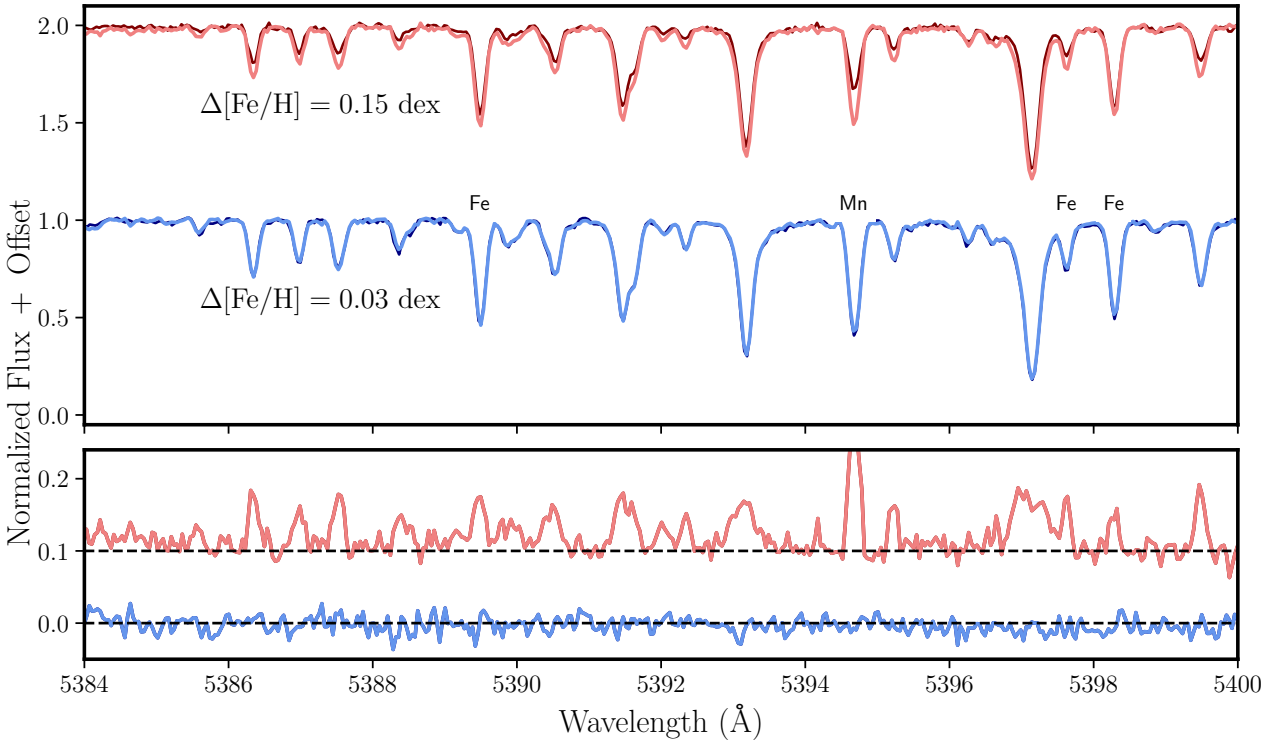

Figure 2. The upper panel shows continuum normalized spectra of both components of two comoving pairs offset by a constant with Δ[Fe/H] of 0.15 dex and 0.03 dex for the upper and lower set of spectra, respectively. Spectral lines which passed the initial quality cut (see Section 3) are also shown in the upper panel. The lower panel shows the difference between the components. Since we only target stellar twins with $\Delta T_{\rm eff} \lesssim 100$ K for both comoving pairs, the differences in the spectra are primarily due to the element abundances of the stars.

close comoving pairs and the far comoving pairs with a 1pc (or 2×10^5 AU) threshold.

It is expected that many of the closest pairs in the sample are gravitationally bound wide binaries with true 3D separations smaller than this distance "resolution" afforded by the *Gaia* parallaxes. Parallax uncertainties effectively stretch these pairs out along the line of sight, in an effect that is analogous to the "fingers of God" distortion in cosmological surveys, where galaxy pairs and clusters are stretched out by redshift uncertainties. For such pairs, the point estimate of the 3D separation from method 1 will dramatically overestimate the true 3D separation. The *projected* separation (which is not subject to inflation by parallax uncertainties) will be much smaller than the point estimate of the 3D separation.

Figure 3 compares the 2D and apparent 3D pair separations for all 33 comoving pairs. The 3D separations are calculated using method 1, as described above. We also show the results separately using astrometry from DR2 and eDR3. At large separations, where the parallax uncertainties are small compared to the parallax differences, the 2D and 3D separations agree within a factor of a few, and difference between the separations calculated using DR2 and eDR3 astrometry are minor. By contrast, pairs with 2D separations less than 10^5 AU fall far below the one-to-one line, with projected separations that are much smaller than the calculated 3D separations. For a majority of these pairs, the apparent 3D separation shrinks between DR2 and eDR3 astrometry. This reflects the fact that parallax uncertainties are smaller in eDR3 data, causing the separation inflation to be less severe. Cross-matching with El-Badry et al. (2021) (E21) shows that almost all of these pairs have a high probability of being gravitationally bound wide binaries,[4] suggesting that their 3D separations are indeed over-estimated due to the parallax errors.

This suggests that the separations of the close comoving pairs are dominated by parallax errors and that even Gaia eDR3 cannot "resolve" their line-of-sight distance difference. Therefore, for close pairs, we instead derive constraints on the 3D separation based on the projected separation, the assumption of random viewing angles, and a prior on the 3D separation distribution of wide binaries. This is describe

[4] In particular, 18 of the 21 pairs in our sample with projected 2D separations below 10^5 AU are in the E21 catalog; these all have a reported chance alignment probability of less than 0.001. None of the pairs with 2D separations above 10^5 AU are in the catalog. The three pairs that have 2D separations below 10^5 AU (and a 3D separation of $\sim 10^5 - 10^6$ AU) and are not in the catalog only narrowly fail the cuts on parallax and/or proper motion consistency required for membership in the E21 catalog and thus may still be bound.

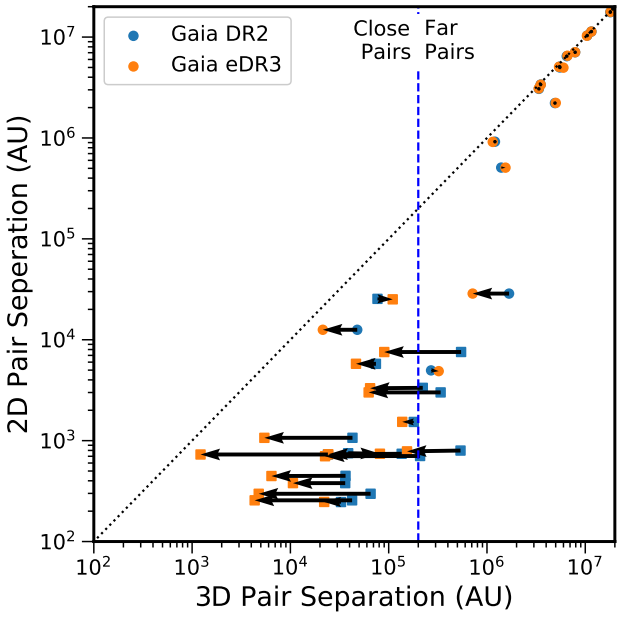

Figure 3. The 2D projected pair separation plotted against the 3D pair separation for both Gaia DR2 (blue) and eDR3 (orange). The square symbols indicate pairs which are in the wide binary catalog from El-Badry et al. (2021), and circles are used otherwise. All separations are calculated directly from Gaia eDR3 astrometry. For a given pair, the grey arrow links the DR2 data to the eDR3 calculation. The blue dashed line indicates our defined boundary separating the close and far comoving pairs. For the far comoving pairs, the parallax error is subdominant. As such, the 2D separations and 3D separations line up. However, for close moving pairs, the parallax error dominates over the separation calculation, and the calculated 3D separation is much larger than the 2D projected separation. Since bound binaries are expected to have smaller separations ($\lesssim 10^5$ AU), this further validates that the parallax errors dominate for the close comoving pairs. Due to this limitation, we impose a geometric prior (Appendix A) when calculating the 3D separation for the close comoving pairs.

in Appendix A. We refer to this method of estimating the 3D separation, which only relies on the projected 2D separation, as "method 2". For method 2, the point estimate and 1σ confidence interval on the 3D separation, r_{3D} are $r_{3D} = 1.12^{+0.49}_{-0.11} \times r_{2D}$, where r_{2D} is the projected separation. Motivation for this expression is given in Appendix A.

With different separation estimators for close pairs (thought to be binaries) and far pairs (thought to be unbound), it is necessary to decide where to draw the line between the two regimes. For simplicity, we use method 2 on all pairs for which the 3D separations calculated using method 1 are less than 2×10^5 AU (dashed blue line in Figure 3). It is possible that a few pairs wider than this (i.e. with $10^5 - 10^6$ AU), which also have projected separations significantly smaller than their calculated 3D separations, are also binaries. Improved parallax uncertainties in future *Gaia* data releases will help determine whether they are bound. But we have checked that separating the bound and unbound pairs with a 10^6 AU threshold leaves most of our qualitative results unaltered.

As most studies usually operate at the projected space instead of the 3D space adopted in this study, when comparing with the literature values (Ramírez et al. (2019), and Hawkins et al. (2020b)), we calculate the 3D separations and velocity differences of their targets with the same process as detailed above. We adopt the latest Gaia eDR3 astrometry and the RV from the literature. RV data was not provided in Ramírez et al. (2019). Hence we used Gaia eDR3 RVs for the Ramírez et al. (2019) data set.

3. STELLAR PARAMETERS AND ABUNDANCES

We use the Brussels Automatic Code for Characterizing High accUracy Spectra (BACCHUS, Masseron et al. 2016) to determine stellar parameters (i.e., $T_{\rm eff}$, log g, [Fe/H], $v_{\rm micro}$) and abundances. An overview of the software is provided below. For a more comprehensive description we refer the reader to Section 2.2 of Hawkins et al. (2015), Masseron et al. (2016), and Appendix A.12 of Smiljanic et al. (2014).

BACCHUS fits observations using spectral synthesis. These spectra were constructed from MARCS model atmospheres (Gustafsson et al. 2008) using `TURBOSPECTRUM` (Plez 2012) for radiative transfer. MARCS models are calculated in 1D LTE. If the surface gravity (log g) is $\geq$ 3.0 dex, plane-parallel models are used, and spherical models otherwise. The atmospheric composition uses solar abundance from Grevesse et al. (2007) scaled by metallicity for most elements. MARCs models use separate abundance estimates for C, N, and O (see Gustafsson et al. 2008, Section 4 for more information)[5]. We use Gaia-ESO line list version 5 (Heiter et al. 2019) for atomic transitions. The line list includes hyperfine structure splitting for Sc I, V I, Mn I, Co I, Cu I, Ba II, Eu II, La II, Pr II, Nd II, Sm II. We also include molecular data for CH (Masseron et al. 2014), C_2, CN, OH, MgH (T. Masseron, private communication), SiH (Kurucz 1992), TiO, FeH, and ZrO (B. Pelz private communication). Fe ionization-excitation equilibrium is used in BACCHUS to derive effective temperature ($T_{\rm eff}$), surface gravity, iron abundance ([Fe/H]), and microturbulent velocity ($v_{\rm micro}$). Other broadening sources (e.g., rotation, instrument resolution, macroturbulence) are modeled by a Gaussian convolution.

Stellar parameters and the convolution kernel size are derived in BACCHUS using the `param` module. We first opti-

[5] Some MARCs models take into account the Galactic trends in [α/Fe] vs [Fe/H]. These models are used for [Fe/H] ≤ -1 dex. However, over the metallicity range of 0 ± 0.3 dex spanned by this sample, such effect is minimal. We thus assume the solar scaling for the α-captured elements for this study.

Table 2. The 3D separations (S) and velocity differences (Δv_{3D}) between comoving pairs. A full machine-readable version is available online. The subscript eDR3 indicates separations calculated solely from Gaia eDR3 astrometry and the spectroscopic RV. As discussed in Section 2.1, the separations calculated this way may overestimate the true separation between the close comoving components. For the subset of comoving pairs suspected to be wide binaries, we invoke a geometric prior based to infer the 3D separations based on the better measured 2D projected separations (Appendix A). We only perform this correction for the close comoving pairs. These separations are denoted with a subscript "geometric". The uncertainty for the geometric separations is asymmetric, so the upper and lower error bars (16 and 84 percentiles) for this separation are listed separately. The results in this paper assumes $S_{geometric}$ for close comoving pairs (i.e., $S_{eDR3} < 2 \times 10^5$ AU) and S_{eDR3} for the far comoving pairs.

Gaia eDR3 ID for Component A	Gaia eDR3 ID for Component B	Identifier	S_{eDR3} (AU)	$\sigma_{S_{eDR3}}$ (AU)	Δv_{3D} (km s^{-1})	$\sigma_{\Delta v_{3D}}$ (km s^{-1})	$S_{geometric}$ (AU)	$\sigma_{lower_{S_{geometric}}}$ (AU)	$\sigma_{upper_{S_{geometric}}}$ (AU)
6160638833832941312	3471119180522314624	CM00	1.1 x 10^6	2.7 x 10^4	0.86	0.05	–	–	–
3613454637229633664	3613454637229634176	CM01	9.0 x 10^4	1.8 x 10^5	1.02	0.08	8.5 x 10^3	8.3 x 10^2	3.7 x 10^3
3639520621950395904	3639520621950395776	CM02	2.2 x 10^4	9.3 x 10^3	1.29	0.04	2.8 x 10^2	27	1.2 x 10^2
5897704951769034368	5897785667103983616	CM03	1.5 x 10^6	1.0 x 10^5	0.93	0.05	–	–	–
6224633983987510528	6224633983987511552	CM04	1.1 x 10^4	1.6 x 10^4	1.71	0.08	4.2 x 10^2	41	1.9 x 10^2
6004256909931771136	6004256802548180736	CM05	1.2 x 10^3	8.6 x 10^3	0.82	0.06	8.2 x 10^2	80	3.6 x 10^2
5877155289930033024	5877155289930029184	CM06	6.5 x 10^4	6.7 x 10^4	0.70	0.06	3.7 x 10^3	3.6 x 10^2	1.6 x 10^3
5798991008295109120	5798991008295120896	CM07	3.2 x 10^5	7.1 x 10^4	1.43	0.07	–	–	–
6214634887804201728	6214634887804233088	CM08	6.4 x 10^3	4.8 x 10^4	0.58	0.04	5.0 x 10^2	49	2.2 x 10^2
6208919660724640896	6208919660723526272	CM09	8.1 x 10^4	3.2 x 10^4	0.79	0.06	8.3 x 10^2	81	3.6 x 10^2

mize for the convolution. The we determine T_{eff} by requiring a null trend,within 1σ of the fit, in Fe I abundance versus excitation potential. We determine log g by enforcing the abundances from Fe I and Fe II lines to agree within the line-by-line rms and v_{micro} by enforcing that there is no trend in iron abundance to reduced equivalent width (i.e., EW/λ). The metallicity is taken as the mean of the Fe I lines relative to the Sun. The parameter fitting uses 94 Fe I lines and 32 Fe II lines, and the details can be found in the full version of Table 3. The reported errors in T_{eff}, log g, and v_{micro} are calculated through the usual propagation of error from the determination of EW of individual lines. We note that, currently, BACCHUS does not estimate the covariances between stellar parameters.

After optimizing the stellar parameters, abundances for 24 elements are measured in BACCHUS with the `abund` module. We measure abundances for the following elements: Li, C, Na, Mg, Al, Si, Ca, Sc, Ti, V, Cr, Mn, Fe, Co, Ni, Cu, Zn, Sr, Y, Zr, Ba, La, Nd, and Eu. The `abund` module synthesizes spectra at different [X/H], fixing the atmospheric model parameters to the best fitting stellar parameters. This model is generated through interpolation of nearby MARCs atmospheres; we determine the abundance for each line by minimizing the unweighted χ^2 of the observed and synthesized spectrum, and we repeat this process for all selected absorption lines for that species. The line list selection is given in Table 3. We select lines based on visual inspection of the synthesis compared with observed spectra for three stars, CM07A, CM11A, and CM25A. We select these stars because they are representative for different atmospheric parameters and rotational broadening. On top of that, for every star in our sample, selected lines must pass an internal quality check to be considered usable for that object. The internal quality check corresponds to a decision tree regarding whether the abundance output is physically plausible and constrained by the trial solutions (see Section 2.2 of Hawkins et al. 2015, for more details on the internal quality check). As a consequence of the internal quality check, the lines with measured abundances may vary between pairs. But we emphasize that for each pair, we adopt the same set of lines for the differential analysis.

We study the abundance differences using both line-by-line (differential) and non-line-by-line (nLBL) "global" methods. Both methods provide similar conclusions; however, the differential method generally leads to better precision because it mitigates systematic errors in the spectral models. We will adopt the abundances derived with the differential method throughout this study. But for completeness, we include results from both approaches in Table 4. For clarity, we denote abundances for individual lines with a subscript i. For example, $[X_i/H]$ indicates an abundance of species X for line i, $\Delta[X_i/H]$ is the difference of species X using the abundance of line i between two stars. Species without subscripts are the overall estimate of the abundance from all corresponding spectral features.

In the differential approach, we compute $\Delta[X_i/H]$ for each transition observed in both stars. The abundance difference is taken as the median of these values (i.e., $\Delta[X/H] = \text{median}(\Delta[X_i/H])$). The median is used instead of the mean because it is more robust against outliers. As for the certainty

Table 3. A portion of our line list selection. A full machine-readable version, including abundances for each star for each line, is available online. The lines used will vary between stars because of the quality checks. χ is the excitation potential, and $\log(A_\chi)$ is the absolute abundance (before subtracting the Solar abundances) derived for this line. The solar abundances adopted are from Grevesse et al. (2007), except where described otherwise in Section 3. Reference keys can be matched with the full citation in Table 7 to determine the origin of the log gf values used.

Identifier	Element	λ (Å)	log gf (dex)	Reference Key	χ (eV)	$\log(A_X)$ (dex)
CM00A	Na I	5682.630	-0.706	GESMCHF	2.102	6.053
CM00A	Na I	5688.200	-0.404	GESMCHF	2.104	6.291
CM00A	Na I	6154.220	-1.547	GESMCHF	2.102	6.181
CM00A	Na I	6160.740	-1.246	GESMCHF	2.104	6.196
CM00B	Na I	5682.630	-0.706	GESMCHF	2.102	6.103
CM00B	Na I	5688.200	-0.404	GESMCHF	2.104	6.311
CM00B	Na I	6154.220	-1.547	GESMCHF	2.102	6.212
CM00B	Na I	6160.740	-1.246	GESMCHF	2.104	6.233
CM01A	Na I	4751.820	-2.078	GESMCHF	2.104	6.558
CM01A	Na I	5682.630	-0.706	GESMCHF	2.102	6.528

estimation, we assume the statistical errors for Δ[X/H], i.e., std(Δ[X$_i$/H])/$\sqrt{\text{number of lines}}$, as the standard error of the mean of the line abundance differences. However, if a single line remains after quality cuts, we take the error as 0.1 dex. This is 1/3 the step size used between trial values in [X/H] when calculating the abundance for each line.

Abundance errors from the uncertainty in $T_{\rm eff}$, log g, and $v_{\rm micro}$ are propagated according to Hawkins et al. (2020b). For each parameter, we perturb the best fit model and derive abundances for this perturbed model atmosphere. The difference between the abundances from the best fit and perturbed model is the error introduced from that parameter. These abundance errors are added in quadrature with the line-by-line statistical errors for Δ[X/H] to determine the total error for an abundance measurement. For simplicity, and due to the BACCHUS code's limitations, we choose to omit the covariances following Hawkins et al. (2020b).

We perform the error analysis on a subset of 30 representative stars distributed evenly over the stellar parameters of our data set. The offsets for $T_{\rm eff}$, log g, and $v_{\rm micro}$ were $\pm$20 K, $\pm$0.1 dex, and $\pm$0.03 km s^{-1}, respectively. The values for $T_{\rm eff}$ and $v_{\rm micro}$ are the median 1σ errors reported by BACCHUS for our sample. We assume a Δ log g= 0.1 dex instead of median reported errors from BACCHUS (0.20 dex) because we find that BACCHUS tend to overestimate the errors of log g due to some outlying Fe II lines. We have separately analyzed these spectra with Bayesian stellar parameter code LoneStar (Nelson et al in prep), which agrees with BACCHUS estimates on all quantities besides the log g errors, which are found to be ~ 0.05 dex. We chose log g errors of 0.10 dex to be conservative since BACCHUS favors larger log g errors. We note however that our comparison between the close comoving pairs, far comoving pairs, and random pairs, is robust and independent of our error estimates.

When we estimate the errors for individual observations, we adopt interpolation by inverse distance weighting (IDW) to estimate the abundance errors resulting from the uncertainties in the stellar parameters for the remainder of the data set. IDW interpolation approximates points outside the reference set by constructing a weighted average of points from the reference sets. These weights are the inverse rms distance. During the interpolation, we transform the stellar parameters onto the interval (-1,1) to weigh each equally. We tested the accuracy of the interpolation using a leave-one-out cross-validation for each element. The average error introduced was typical $< 2\%$ of the true errors calculated for that particular star. Sr and Eu were the only two elements with larger relative errors at $\lesssim 5\%$. Nonetheless, these errors are at least one order of magnitude below the total error budget for each element and are therefore negligible.

Table 4 summarizes the derived stellar parameters and abundance measurements and uncertainties in this study. In addition to the total abundance errors, we also report the errors from the individual errors contributed by the stellar parameter error propagation and the line-to-line scatter of Δ[X/H], respectively. The stellar parameters are the main source of uncertainty. For 23 elements, the stellar parameters account for $> 90\%$ of total error. For Sr, the stellar parameters accounting for $\sim 70\%$ of the total errors. Of the remaining species, Li and Eu typically only have a single line measured and are therefore subjected to the 0.1 dex error floor on the abundance scatter. Only in these rare cases, the "line-to-line" error is more dominant than the stellar parameters' uncertainty. Finally, for completeness, although not shown, the nLBL abundances and errors are also provided in the full machine-readable table.

4. RESULTS

As discussed in the introduction, this paper's main goal is to assess whether or not the comoving pairs in this study, especially for the far comoving pairs, are conatal systems. Since conatalitly cannot be assessed directly outside star-forming regions, we resort to studying the chemical homogeneity (i.e., Δ[X/H]). Figure 4 displays the difference in metallicity between comoving pairs (blue) as a function of pair separation. Although not shown, similar trends are seen for the majority of the elements studied.

For comparison, we also include the wide binaries results from Ramírez et al. (2019), and Hawkins et al. (2020b). We note that Ramírez et al. (2019) includes results for 12 systems, 11 of which are from other studies (i.e., Ramírez et al. 2010; Liu et al. 2014; Mack et al. 2014; Ramírez et al. 2014;

Table 4. Stellar parameters and elemental abundances derived from BACCHUS. A and B subscripts denote the two components from the comoving pairs. ξ denotes the microturbulence. The electronic table contains measurements from nLBL and differential methods. All the differential measurements (e.g., $\Delta[\mathrm{Fe/H}], \sigma_{\Delta[\mathrm{Fe/H}]}$) are measured with differential method. But we also provide individual estimates of each component with the nLBL method, indicated with the subscripts A and B. By definition, the differential analysis only applies to the differences of the two components, and there will be no individual values with the differential method. The full table also separately lists the errors from differential stellar parameters (denoted with a subscript θ) and the statistical line-to-line scatter (denoted with a subscript line), but below we only show the total errors (adding in quadrature). ΔRV refers to the difference in radial velocity measured from our observations and Gaia eDR3. The large ΔRV column indicates whether the system was flagged for potentially being a hierarchical triplet with an unresolved binary.

Component A ID	Component B ID	Identifier	Large ΔRV	T_{eff_A} (K)	$\sigma_{T_{\mathrm{eff}_A}}$ (K)	T_{eff_B} (K)	$\sigma_{T_{\mathrm{eff}_B}}$ (K)	$\log g_A$ (dex)	$\sigma_{\log g_A}$ (dex)	$\log g_B$ (dex)	$\sigma_{\log g_B}$ (dex)	ξ_A (km s^{-1})
6160638833832941312	3471119180522314624	CM00	False	5809	9	5934	65	4.53	0.30	4.65	0.41	1.22
3613454637229633664	3613454637229634176	CM01	False	6058	25	6002	56	4.29	0.16	4.14	0.28	1.30
3639520621950395904	3639520621950395776	CM02	False	5962	11	5966	11	4.38	0.22	4.41	0.23	1.06
5897704951769034368	5897785667103983616	CM03	False	6036	37	6121	28	4.34	0.22	4.28	0.21	1.31
6224633983987510528	6224633983987511552	CM04	False	5763	26	5822	11	4.51	0.14	4.50	0.20	0.90

σ_{ξ_A} (km s^{-1})	ξ_B (km s^{-1})	σ_{ξ_B} (km s^{-1})	Δ[Fe/H] (dex)	$\sigma_{\Delta[\mathrm{Fe/H}]_{\mathrm{Total}}}$ (dex)	Δ[Na/H] (dex)	$\sigma_{\Delta[\mathrm{Na/H}]_{\mathrm{Total}}}$ (dex)	Δ[Mg/H] (dex)	$\sigma_{\Delta[\mathrm{Mg/H}]_{\mathrm{Total}}}$ (dex)	Δ[Al/H] (dex)	$\sigma_{\Delta[\mathrm{Al/H}]_{\mathrm{Total}}}$ (dex)	Δ[Si/H] (dex)
0.04	1.31	0.05	0.04	0.02	0.03	0.02	0.02	0.02	-0.02	0.02	0.01
0.04	1.33	0.04	0.02	0.02	0.05	0.02	0.03	0.02	0.03	0.01	0.01
0.04	1.05	0.04	0.00	0.02	0.00	0.02	0.01	0.02	-0.02	0.01	0.01
0.04	1.34	0.04	-0.08	0.02	-0.11	0.02	-0.06	0.02	-0.12	0.02	-0.08
0.04	0.99	0.04	-0.01	0.02	-0.00	0.03	0.01	0.01	0.00	0.01	-0.03

$\sigma_{\Delta[\mathrm{Si/H}]_{\mathrm{Total}}}$ (dex)	Δ[Ca/H] (dex)	$\sigma_{\Delta[\mathrm{Ca/H}]_{\mathrm{Total}}}$ (dex)	Δ[Sc/H] (dex)	$\sigma_{\Delta[\mathrm{Sc/H}]_{\mathrm{Total}}}$ (dex)	Δ[Ti/H] (dex)	$\sigma_{\Delta[\mathrm{Ti/H}]_{\mathrm{Total}}}$ (dex)	Δ[V/H] (dex)	$\sigma_{\Delta[\mathrm{V/H}]_{\mathrm{Total}}}$ (dex)	Δ[Cr/H] (dex)	$\sigma_{\Delta[\mathrm{Cr/H}]_{\mathrm{Total}}}$ (dex)	...
0.02	-0.01	0.05	0.04	0.06	0.07	0.03	0.09	0.04	0.05	0.03	...
0.02	0.01	0.03	0.02	0.05	0.02	0.03	0.01	0.03	0.06	0.03	...
0.02	-0.02	0.04	0.01	0.06	-0.00	0.03	-0.01	0.04	0.01	0.03	...
0.02	-0.06	0.03	-0.10	0.05	-0.07	0.03	-0.09	0.04	-0.09	0.03	...
0.03	-0.00	0.05	-0.04	0.07	0.00	0.03	0.05	0.04	0.03	0.04	...

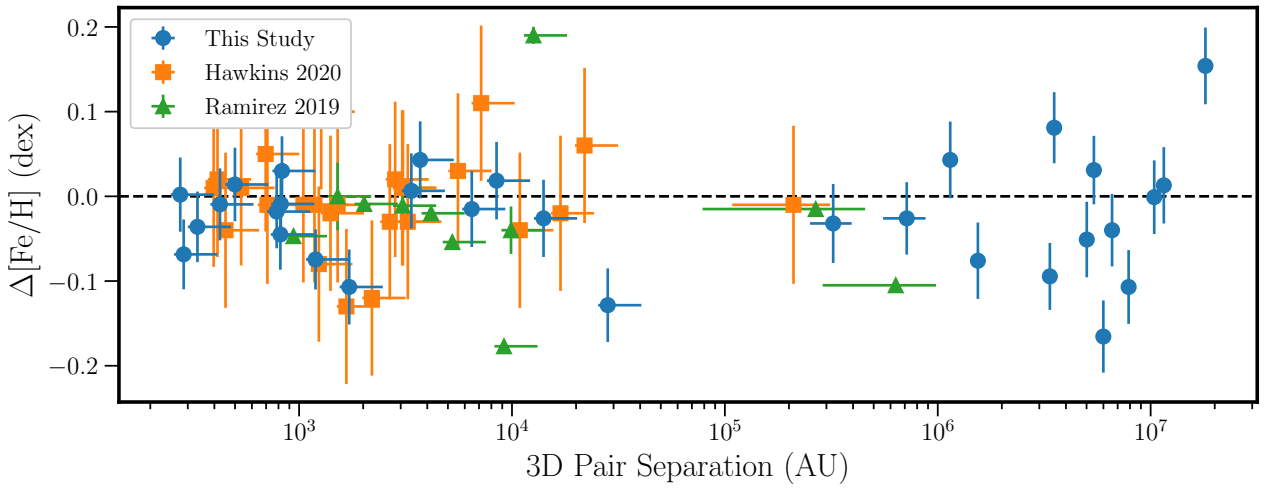

Figure 4. A comparison of the comoving pairs (blue) with similar works on wide binaries. Separation errors for pairs with separations $> 10^6$ AU are essentially negligible and smaller than the symbol size. Our close comoving pairs (i.e., wide binaries) have a similar degree of chemical homogeneity to the literature values. Far comoving pairs (pairs with separations $> 2 \times 10^5$ AU) are also chemically homogeneous in [Fe/H], with a scatter of < 0.1 dex, albeit being slightly less homogeneous than close comoving pairs.

Tucci Maia et al. 2014; Teske et al. 2016; Saffe et al. 2016; Mack et al. 2016; Saffe et al. 2017; Reggiani & Meléndez 2018; Oh et al. 2018). In the remainder of the paper, we will exclude the system from Mack et al. (2014) from comparisons because it appears to be a hierarchical triplet with an unresolved binary, and use Ramírez et al. (2019) as a shorthand for the remaining 11 systems. We note that since the sample Ramírez et al. (2019) is a heterogeneous sample, the comparison with Hawkins et al. (2020b) might be more relevant. Furthermore, the samples in Hawkins et al. (2020b) have spectra with spectra and were analyzed in the same way as this study. We also compare our data to Andrews et al. (2019); however, they did not provide individual measurements, so our comparison with this work is limited to summary statistics.

As previously discussed, we split our comoving sample into the close (i.e., primarily wide binaries) and far comoving pairs to compare with these works. Close comoving pairs are defined as those having separations below 1 pc, i.e. 2×10^5 AU, (with 17 pairs in this study), and far comoving pairs have separations above 1 pc (14 pairs). For the close pairs, we use the geometric prior when calculating the separations (see Section 2.1) because the parallax error dominates. Our close comoving pairs sample (i.e., wide binaries) show a similar degree of chemical homogeneity as other studies on wide binaries with a dispersion of 0.05 dex in Δ[Fe/H], which is expected. Compared to the close comoving pairs, we find that the far comoving pairs are less chemically homogeneous, with a Δ[Fe/H] dispersion of 0.08 dex; however, the far comoving pairs are substantially more homogeneous than the random pairs (0.23 dex), which we will further explore in the next section. Table 5 summarizes the scatter in Δ[Fe/H] comparing our data with prior works.

4.1. *Chemical Homogeneity of Comoving Pairs*

To contextualize how homogeneous our comoving population is, we simulate pairs of random field stars. In a similar fashion to Hawkins et al. (2020b), we create a set of random pairs by assigning every star to another star, which is not its comoving partner. Since the comoving stars are selected to be stellar twins, for better comparison, we create random pairs which minimize the difference in $T_{\rm eff}$ and log g (labeled $T_{\rm eff}$/log g pairs) to mitigate systematic effects. Since $T_{\rm eff}$ and log g have different units, when minimizing the difference, we divide both quantities by the standard deviation of the pairwise difference for all non-comoving pairs of stars in our sample. The random pairs are shown in Figure 5. Across all elements, the average dispersion in Δ[X/H] for the random pairs is 0.24 dex, significantly larger than the dispersion of both the close comoving pairs (0.05 dex) and the far comoving pairs (0.10 dex).

	median $\lvert\Delta$[Fe/H]$\rvert$ (dex)	std Δ[Fe/H] (dex)
Wide Binaries		
Hawkins et al. (2020b)	0.02	0.05
Ramírez et al. (2019)	0.04	0.09
Andrews et al. (2019)	-	0.04
close comoving pairs	0.03	0.05
Unbound pairs		
far comoving pairs	0.05	0.08
random pairs	0.16	0.23

Table 5. A comparison of the Δ[Fe/H] scatter for our study and three other studies on wide binaries. Andrews et al. (2019) only provides standard deviation without giving the individual measurements, which prohibits us from calculating the median of the absolute difference. Andrews et al. (2019) provides two values for the scatter in Δ[Fe/H], one for the entire sample (0.08 dex) and the other (0.04 dex) for wide binaries with $\Delta T_{\rm eff} <$ 100 K. We only state the latter as it is more relevant to this study. We caution that Ramírez et al. (2019) is a heterogeneous sample of several studies. As such, it could incur a large scatter due to different systematics from these studies, the comparison to the other studies might be less direct.

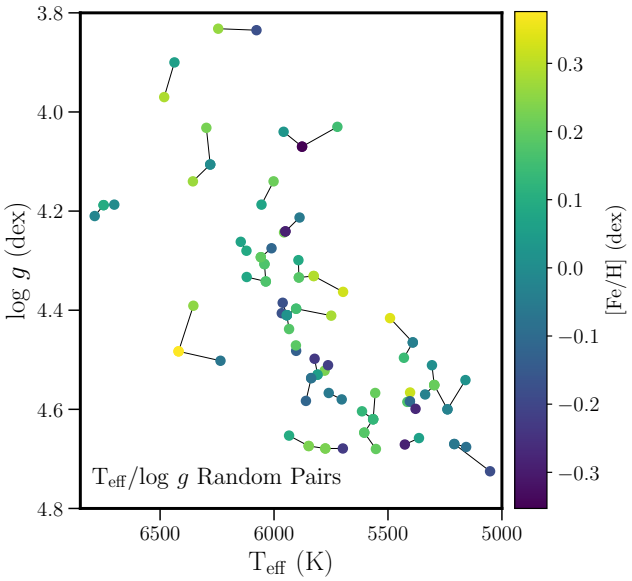

Figure 5. The stellar parameters of the simulated random field pairs in this study. To simulate unrelated pairs of field stars and compare that to the comoving pairs, we assign a partner based on the nearest star in stellar parameter space, which is not its comoving counterpart. The black lines connect paired stars by minimizing the distance in $T_{\rm eff}$ and log g. A single star may be paired with multiple partners. This was allowed because we want to prevent pathological assignments where two stars are paired over large distances because all intermediates are unavailable, artificially inflating systematic uncertainties.

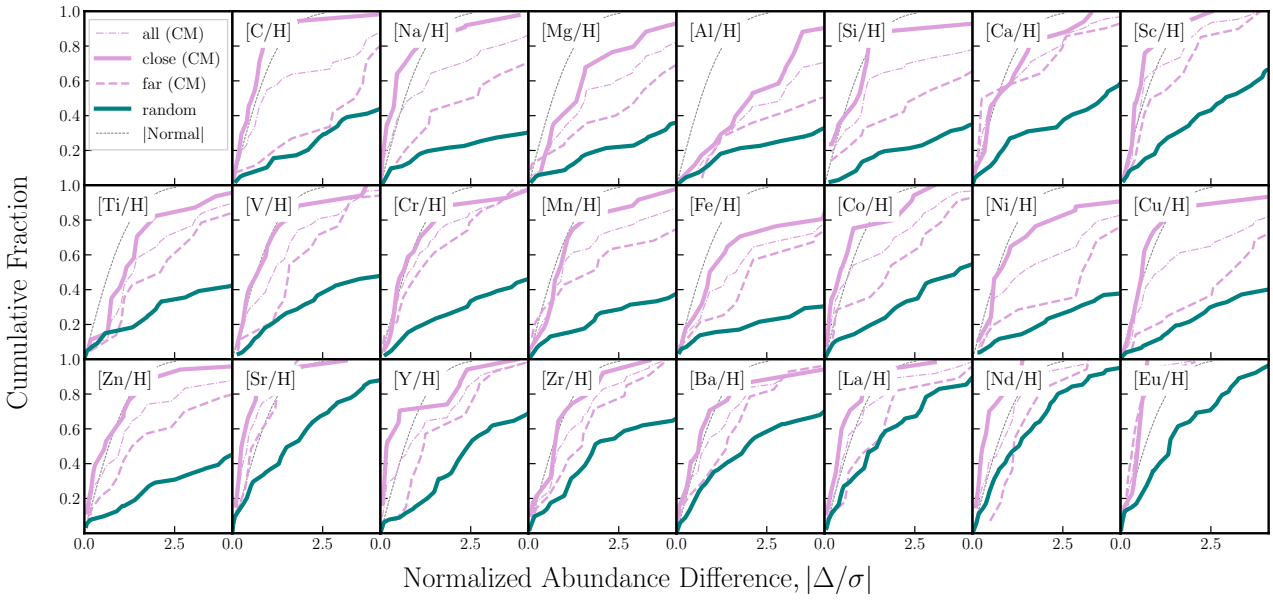

Figure 6. The distribution of difference in elemental abundances normalized by their uncertainties. The comoving pairs are divided into three groups (the entire comoving sample; violet thin dashed line), close (violet thick solid line), and far (violet dashed line, medium width). The thin black line indicates an expected distribution if the scatter in abundance differences between comoving pairs were explained by the measurement uncertainties. The solid teal line indicates the distribution for the random pairs. The close comoving pairs are more chemically homogeneous than the random groups and generally approaches a distribution consistent with the observed spread being only a result of measurement errors. The far comoving pairs are less chemically homogeneous than the close comoving pairs. However, they are generally more chemically homogeneous than the random pairs, indicating a mixed population of conatal pairs and chance alignments.

To better illustrate the difference in chemical homogeneity between these groups, similar to Andrews et al. (2019), we visualize the homogeneity of our sample using $|\Delta[\mathrm{X/H}]|/\sigma_{\Delta[\mathrm{X/H}]}$, which will be abbreviated as Δ/σ. The Δ here is the difference in elemental abundances between the two components, and the σ is the quadrature sum of the uncertainties from the two components. Figure 6 shows the cumulative distribution function (CDF) of Δ[X/H] normalized by the measurement error for the comoving pairs (violet/solid and dashed) and random pairs (teal/solid). For reference, each panel includes the CDF of Δ/σ drawn from the unit Gaussian – i.e., what a chemical homogeneous would look like at the level of our current measurement uncertainties (assuming that our uncertainty estimations are accurate).

There is a clear difference in the random pairs' distribution and comoving pairs, both close and far, largely attributed to the larger chemical dispersion seen in the random pairs. The difference in the CDF between the comoving and random pairs also varies between elements. This variation is primarily caused by the difference in our measurement precision for those elements. On the one hand, for better-measured elements, such as Fe, Mg, Al, and Si, the comoving pairs exhibit a more distinct chemical homogeneity than the random pairs. On the other hand, unsurprisingly, for less well-measured elements, the difference in chemical homogeneity is less distinct, as shown in the CDFs for La, Nd, and Eu. We do not include Li in this plot because its surface abundance has a strong dependence on effective temperature and is therefore not a useful indicator for conatality (see Gray 2008; Ramírez et al. 2012; Hawkins et al. 2020b).

For most elements, the close comoving pairs are consistent with a chemically homogeneous distribution at our measurement precision, with the CDF for 16 elements exceeding 96% by $\Delta/\sigma = 4$. In contrast, the random pairs are less homogeneous, with the CDF for 13 elements $\lesssim 50\%$ at $\Delta/\sigma = 4$.

As already seen in Fig. 4, the far comoving pairs are more heterogeneous than the close comoving pairs for most elements, albeit still being more homogeneous than the random pairs. The slightly larger chemical inhomogeneity is unsurprising because we expect some of the far comoving pairs might be contaminated by chance alignment pairs (e.g., Kamdar et al. 2019a), which we will quantify in the next section.

In this study, we focus on the abundance [X/H] instead of the abundance ratio [X/Fe]. However, all elements correlate with iron in [X/H]. Therefore, the difference between random and close comoving pairs in Δ/σ for [X/H] may only reflect a metallicity difference. While [X/H] (or metallicity alone) are tell-tale signs of conatality (or at least co-eval), studying the abundance ratio [X/Fe] might, in principle, constitute a more stringent test and might reveal subtle physics.

Although not shown, we tried to examine Δ/σ for [X/Fe][6]. We find little difference between the comoving and random pairs of stars in the [X/Fe] space. This is not unexpected because the residual variance in [X/Fe] is much more subtle than in [X/H]. For example, Ting & Weinberg (2021) shows that when one subtracts the mean chemical track, the residual correlation in [X/Fe] is small, with signal $\lesssim 0.01 - 0.02$ dex. Therefore, to see such a signal, we would need to measure [X/Fe] better than ~ 0.01 dex. With the current pipeline adopted in this study, we found that achieving 0.01 dex remains challenging. Therefore, we only focus on [X/H]. Future studies with even higher quality spectra and/or better analysis will be needed to shed light on these subtle variations.

4.2. *Conatal Fraction for Separations* $> 2 \times 10^5$ *AU*

The close comoving pairs (wide binaries) at separations below 2×10^5 AU are commonly believed to be conatal as chance capture is unlikely. However, beyond such separation, the conatality for the far comoving pairs remains unexplored. Armed with our high-resolution spectroscopic data from these pairs, in this section, we will constrain how conatal the far comoving pairs with separations $> 2 \times 10^5$ AU are relative to the close comoving pairs. Showing the conatality of far-comoving pairs can have far-reaching consequences; if these comoving pairs are chemically homogeneous and conatal, this would significantly expand the sample of calibrators beyond open clusters and wide binaries.

As we have seen in the previous section, these far comoving pairs are more heterogeneous than the close comoving pairs/wide binaries but more chemically homogeneous than the random pairs. One explanation for the slightly larger chemical inhomogeneity is that the far comoving pairs are a mixture of conatal pairs and chance alignments. The interlopers create a tails of large $\Delta[\mathrm{X/H}]$. If that is the case, we should be able to constrain the conatality fraction through these far-comoving pairs' chemical homogeneity, which is what we will attempt next.

We only model Δ [Fe/H] because iron has the most precise measurements of any element in our sample, and, as we have argued, most elemental abundances only trace [Fe/H] at the current precision. The basic idea is that, if the Δ [Fe/H] of the far comoving pairs are contributed by the two populations – a conatal population that resembles the wide binaries population and the random pairs interlopers, we would expect the distribution of Δ [Fe/H] would also be a mixture of the two. More specifically, we model the PDF of $|\Delta[\mathrm{Fe/H}]|/\sigma_{\Delta[\mathrm{Fe/H}]}$ (or in short, Δ/σ, in the following) for the far comoving pairs as a mixture model using the weighted average of the close comoving pairs' Δ/σ PDF and the random pairs' Δ/σ PDF. The best-estimated weight signifies the fraction of pairs consistent with the close comoving pairs among the far comoving populations, hence its conatal fraction. Due to our small sample size (~ 10 pairs), we expect considerable uncertainty for estimating the conatal fraction because of the sampling noise. Therefore, to properly model the sampling noise, we also estimate the uncertainty of the estimated conatal fraction by bootstrapping the sample.

Operatively, first, we sample, with replacement, the data distribution of Δ/σ for the close, far, and random pairs. The distributions of points drawn from the close comoving pairs and random pairs are then separately approximated as normal distributions through maximum likelihood estimation (MLE). Subsequently, we fit for the weight of the far comoving pairs distribution, also through MLE, assuming that the Δ/σ distribution of the far comoving pairs is a weighted mixture of the ones determined for the close moving pairs and the random pairs. The bootstrapping process is repeated 1000 times. The bootstrapping produces a distribution of weights. The median and standard deviation are taken as the best estimate and uncertainty of the conatal fraction, respectively.

In Figure 7 we demonstrate the nominal fit without the replacement. For this estimate, we only consider comoving pairs with separations $2 \times 10^5 - 10^7$ AU, excluding the three pairs with separations $> 10^7$ AU, leaving us with 11 pairs (out of 14 pairs). As we will see in the following, these three pairs are clearly interlopers (based on predictions from simulations). The Δ/σ CDF of the close moving pairs is shown in violet, the far comoving pairs in violet/black, and the random pairs in teal. A continuum of mixture model CDFs is displayed in the background as a blue/yellow gradient ranging from close:random ratios of 1:4 to 9:1, or equivalently, a conatal fraction 20%-90%. Besides, we highlight some fractions with white dotted contours to guide the reader. We find the conatal fraction for the 11 far comoving pairs with separations $2 \times 10^5 - 10^7$ AU to be $73 \pm 22\%$. In short, our result implies that $\sim 75\%$ of the far comoving pairs are conatal based on their metallicity measurements.

5. DISCUSSION

Conatal stars are the central hallmarks in modern-day Galactic Archaeology. Absolute standards are hard to come by (Jofré et al. 2014; Blanco-Cuaresma et al. 2014b; Heiter et al. 2015), but if we know the two stars are conatal, the two components serve as each other references. This is why open clusters and wide binaries have always been the golden calibrators to refine stellar models, to study exoplanets, gas mixing, and to calibrate surveys. More recently, the high precision astrometry measurements from Gaia now allow us to identify wide binaries at high fidelity, which further propels the study of wide binaries. However, most studies of

[6] For this test, we minimized the difference in T_{eff} and [Fe/H] when simulating the random field pairs to find pairs of stars with the same metallicity.

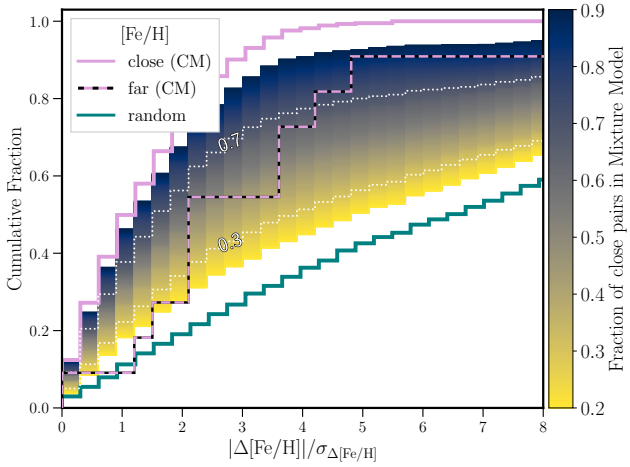

Figure 7. The normalized chemical homogeneity CDFs for different populations in this study. The CDF from the close comoving pairs/wide binaries is plotted in the bold violet line and the random field pairs in the bold teal line. The colored region represents a mixture model of the close and random pairs using different mixing ratios. The far comoving pairs (violet/black dashed) with separations of $2 \times 10^5 - 10^7$ AU is best modeled with a mixture with a 73%/27% ratio of the close comoving pairs versus the random pairs. If all close comoving pairs are conatal, the chemistry of stars reveals that about 73% of the far comoving pairs are conatal.

wide binaries (e.g., El-Badry et al. 2021) often assume a dichotomy between wide binaries and chance alignments, and this picture is clearly too simplistic. Simulations (Kamdar et al. 2019a,b) have suggested comoving stars from disrupted star clusters could have a high probability of being conatal out to separations of $\mathcal{O}(10^6)$ AU. If this is correct, unbound comoving stars could be used in similar ways as wide binaries and open clusters. Based on modeling of Gaia data by Ting et al (in prep), we expect to find roughly 3300 conatal pairs with 3D separations $\lesssim 2 \times 10^6$ AU (10 pc) and $\Delta v_{3D} < 2$ km s^{-1}.

In this study, we perform the first homogeneous study of comoving pairs that span five orders of magnitude in separation. A homogeneous sample allows us to study the chemical homogeneity of the comoving stars with different separations consistently. We found that the close comoving pairs with separations $< 2 \times 10^5$ AU have a Δ[Fe/H] scatter of 0.05 dex. These values are comparable to the typical values seen in open clusters and other wide binaries studies. In particular, we opt to perform the same analysis as Hawkins et al. (2020b). With similar resolution and SNR, Hawkins et al. (2020b) showed a dispersion of 0.05 dex for wide binaries, largely consistent with this study. On top of that, we show that the abundance differences for almost all elements are consistent with the measurement uncertainties, further validating that close comoving pairs/wide binaries are conatal. We note that some of the Δ[Fe/H] scatter seen in the systems from Ramírez et al. (2019) could be a consequence of a selection effect. Many of those systems were published in the context of planet engulfment signatures. Consequently, the systems which show the engulfment signals (e.g., Kronos and Krios Oh et al. 2018), will also have larger metal differences. Since exoplanet accretion changes the surface abundances, these systems may not be representative of the true chemical homogeneity of conatal systems.

More importantly, our study expanded on previous works by also examining comoving pairs with separation $> 10^6$ AU. The key result of our study is that comoving pairs at these larger separations are still significantly more chemical homogeneous than the random pairs, albeit with a slightly larger dispersion in chemistry, with a scatter Δ[Fe/H] of 0.09 dex. The random pairs have a scatter of 0.23 dex. If we assume that the far comoving pairs are comprised of both the conatal stars and chance alignments, we estimate that about $73 \pm 22\%$ of pairs with separations $2 \times 10^5 - 10^7$ AU are conatal.

A caveat with this estimation is that, in this study, we select stellar twins with a median $|\Delta T_{\rm eff}|$ of 105 K. The selection of stellar twins enables the mitigation of any potential systematics in terms of the spectral modeling by performing a line-by-line differential study. Conveniently, from their construction, the simulated random pairs have a smaller difference in stellar parameters (with a median $|\Delta T_{\rm eff}|$ of 47 K), so we would expect these systematic effects to be similar or weaker in the random population. However, for completeness, we investigated whether or not the more significant dispersion in metallicity difference is real or simply due to systematic errors when deriving abundances from stars that are more different in stellar parameters.

To dissect that, we looked into any potential biases in Δ[Fe/H] as a function of the difference in stellar parameters. We found weak trend between Δ[Fe/H] and $\Delta T_{\rm eff}$, $\Delta \log g$, and $\Delta v_{\rm micro}$. For example, Δ[Fe/H] shows a positive correlation with $\Delta T_{\rm eff}$, with a gradient of 2.3×10^{-4}dex K^{-1}. We attempted to account for that by fitting a multivariate linear regression between Δ[Fe/H] as a function of $\Delta T_{\rm eff}$, $\Delta \log g$, and $\Delta v_{\rm micro}$. We found that this process typically leads to a correction of 0.002 dex in Δ[Fe/H], which is negligible for our study. We conclude that it is unlikely the differences in chemistry between the comoving and random pairs are attributable to this correlation. We opted not to remove these correlations because it is hard to determine the exact causal direction of this correlation.

Recall that, the observations in this study are largely motivated by the simulation from Kamdar et al. (2019a), in which the authors argued that far comoving pairs are also conatal. So, how does our study compare with the simulation? In Figure 8, we compare our data with the Kamdar et al. (2019a) simulation. Our comoving pairs are represented as

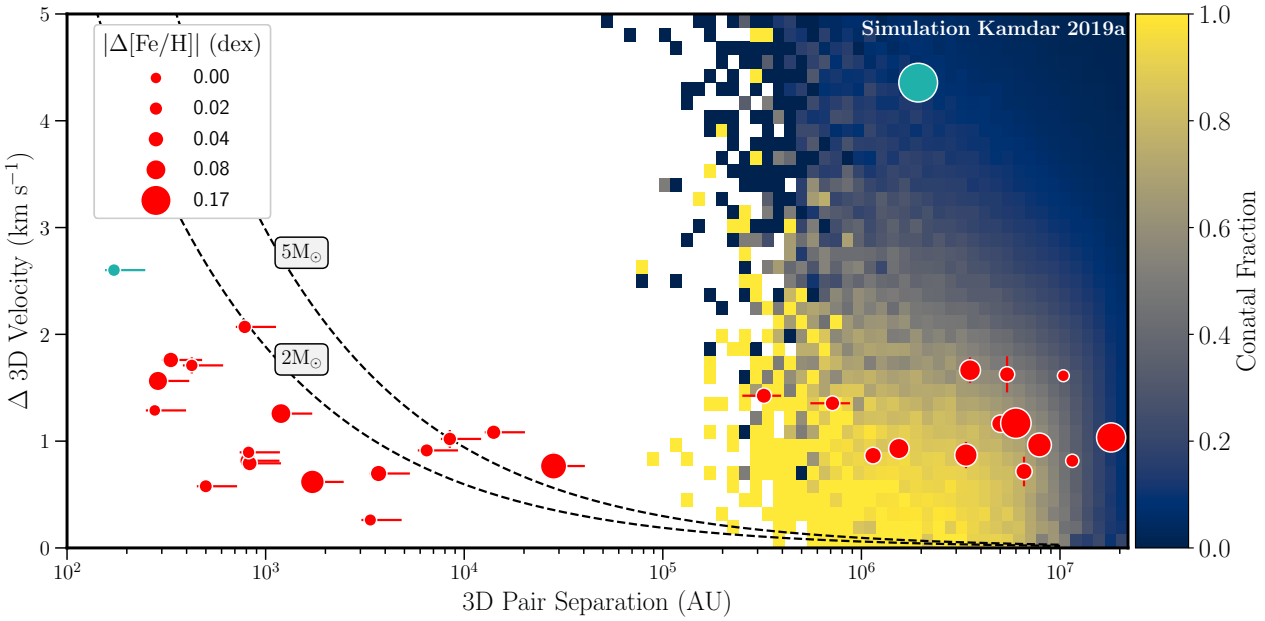

Figure 8. A comparison of our main sample (red circles) with the theoretical predictions from simulation (Kamdar et al. 2019a). The symbol sizes are scaled relative to the two stars' metallicity differences. A smaller metallicity difference indicates a larger likelihood of being a conatal pair. The background shows the expected conatal fraction according to the simulation. The simulation does not include wide binaries and therefore does not extend to separations below 10^5 AU. The black dashed contours on the left indicate the maximum velocity difference a bound system could have with a given total mass, assuming equal-mass companions and no unseen tertiaries. Our data show excellent agreement with the simulation, with smaller metallicity differences within the predicted locus of conatal stars and more considerable metallicity differences outside the locus. We include two systems (bluegreen) that have velocity difference > 2 km s^{-1} as references. The first is a system with a velocity difference of 2.5 km s^{-1} and a separation of 2×10^2 AU, this is well within the parameter space for a binary system and is likely conatal. The second has a larger spatial separation (2×10^6 AU) and a velocity difference greater than 4 km s^{-1}. The simulation predicts that such a pair is likely a chance alignment. The abundance differences of these two pairs concur with these expectations.

red circles, and the symbol size shows the metallicity difference of the two stars for individual pairs. The black dashed lines indicate the escape velocity of bound systems, assuming equal-mass companions, and with the total masses of $2M_\odot$ and $5M_\odot$ respectively. The simulation does not extend below 10^5 AU because the simulations did not attempt to model wide binaries (only disrupted star clusters).

Our results exhibit excellent agreement with the simulations; our sample shows a high degree of chemical homogeneity in the regime where the simulations predict to have a high conatality rate (the region in yellow). In the phase space regime where chance alignments should dominate (in blue background), our observations also show the largest metallicity differences (largest symbol sizes). Also more quantitatively, the simulation predicts that $\sim 80\%$ of comoving pairs are conatal provided $\Delta v_{3D} < 2$ km s^{-1} and the pair separation is between $2 \times 10^5 - 10^7$ AU . Our conatality fraction estimate of $73 \pm 22\%$ for separations is well aligned with the simulation's predictions.

On top of that, besides our (31 pairs of the main sample), as discussed in the target selection, we also observed two pairs with large Δv_{3D} (> 2 km/s) as the control sample. One of the two pairs has a spatial separation of 2×10^2 AU. Even though they are not within $\Delta v_{3D} < 2$ km s^{-1}, this pair is clearly a bound binary, and therefore is conatal. The other pair has a large separation (2×10^6 AU) *and* a large velocity difference (4 km s^{-1}). The simulation predicted this pair is firmly a chance alignment pair as disrupted star cluster members are unlikely to exhibit such a large velocity difference. As shown in Fig. 8, our abundance measurement indeed concurs with this picture, the former has a metallicity difference that is typical of that of wide binaries, and the latter has a dispersion of 0.24 dex, consistent with what we expect from a random pair. With this in mind, we caution that all the results presented in this study, including the conatal fraction, only strictly applies to stars with $\Delta v_{3D} < 2$ km s^{-1}.

While the agreement is encouraging, due to the small sample size, unfortunately, we could only settle on two separation bins – those with separations $< 2 \times 10^5$ AU and those with $2 \times 10^5 - 10^7$ AU. It is clear from the simulation that there is no sharp transition between the conatal to random pairs. But instead, the regime of purely conatal pairs transitions gradually toward the regime dominated by chance alignments. The transition depends critically on many Galactic properties, including how stars form and disperse and the cluster mass function. On top of that, as explored in Kamdar et al.

Threshold (AU)	Conatal Fraction
10^5	$52 \pm 26\%$
2×10^5	$73 \pm 22\%$
10^6	$61 \pm 31\%$

Table 6. This table details the effects of using different thresholds for the close and far pairs. We always assume an upper separation threshold of 10^7 AU for the far comoving pairs.

(2019a), the number density of comoving stars provide telltale signs on the number density of Galactic perturbers, such as giant molecular clouds in the Milky Way disk, as they disrupt comoving pairs. In short, understanding this transition with critical and refining this boundary region with a larger sample will no doubt shed insights into the formation and dispersion of star clusters and other substructures in the Milky Way.

The exact value of the division between close pairs (i.e., wide binaries) and far pairs (presumed unbound) is somewhat arbitrary. Bound pairs are not expected to exist at separations beyond 1-2 pc, because at these separations the Galactic tidal field is stronger than the internal acceleration within a binary (e.g. Jiang & Tremaine 2010). At separations of order 1 pc, there will always be some ambiguity between still-bound and recently-dissolved pairs, and the reliability with which bound pairs can be identified will depend on the precision of the astrometry (e.g. El-Badry et al. 2021). A possible alternative to adopting a strict threshold at $S_{eDR3} = 2 \times 10^5$ AU would be to only consider as binaries pairs that are members of a predetermined wide binary catalog, such as the one produced by El-Badry et al. (2021). The disadvantage of this approach is that such catalogs are generally not 100% complete. Increasingly precise astrometry form future *Gaia* data releases will make it possible to classify pairs with separations of order 1 pc more reliably. For now, we note that because of our small sample size, our estimates of the conatal fraction are considerable and are dominated by small number statistics. Small changes in the adopted boundary between close and far pairs thus lead to changes in our inferred conatal fraction that are comfortably within our reported uncertainties. For completeness, we provide a summary of the effects of choice of separations for the far pairs in Table 6.

Finally, in this study, we assume that the difference in chemical homogeneity for the far comoving pairs compared to the close conatal pairs stems from random pairs interlopers. However, another potential source for these differences in chemical homogeneity could be from the ISM being less mixed at the largest scale. At the $\mathcal{O}(10^7)$ AU scale, ISM can have abundance scatter of up to 0.3 dex (e.g. Sanders et al. 2012). If stars formed in a poorly mixed cloud, they might inherit this scatter. We deem such a scenario unlikely because hydrodynamic simulations have found that, in a single star-forming region, even small amounts of turbulence can cause a factor of five reductions in abundance to scatter in stars compared to the progenitor ISM (Feng & Krumholz 2014). And this chemical reduction scatter applies to scales large as $\mathcal{O}(10^6) - \mathcal{O}(10^7)$ AU, the maximum scale probed in this study.

That said, if the stars formed in a filamentary structure at different star-forming regions, the ISM might be less well mixed. For example, Hawkins et al. (2020a) argue Pisces-Eridanus stellar stream could have been produced from a stellar filament. They find a metallicity range of ~ 0.2 dex for the stream, which is consistent with our metallicity difference in the far comoving pairs. If the chemical inhomogeneity is due to the ISM physics instead of random interlopers, our conatality fraction estimated would be a conservative limit. The far comoving pairs would have an even higher conatal fraction than what was is inferred here.

6. SUMMARY

We obtained a homogeneous sample of high-resolution ($R \simeq 40000$), high SNR (~ 150 per pixel) observations of 62 FG-type stars residing in 31 comoving pairs with separations that span five orders of magnitude in separation, between 10^2 AU to 10^7 AU. Previous studies mostly restricted to wide binaries with separation $< 10^6$ AU, and we investigate if the (unbound) comoving stars with separations $= 2 \times 10^5 - 10^7$ AU are conatal. We measured the stellar atmospheric parameters and chemical abundances for 24 species, including covering the different nucleosynthetic pathways. The derived elemental abundances: Li, C, Na, Mg, Al, Si, Ca, Sc, Ti, V, Cr, Mn, Fe, Co, Ni, Cu, Zn, Sr, Y, Zr, Ba, La, Nd, and Eu.

We separate our sample into the classical wide binaries regime (i.e., close comoving pairs with separations $< 2 \times 10^5$ AU), the far comoving pairs (separations $> 2 \times 10^5$ AU), as well as the random field pairs created through random pairings of our observations. We find the wide binaries are significantly more chemically homogeneous than field stars in [X/H] (see Figure 6) with a typical scatter in Δ[Fe/H] of 0.05 dex. Our results agree with previous works on wide binaries and comoving pairs (see, e.g., Andrews et al. 2019; Hawkins et al. 2020b). For most elements in the close comoving pairs, the dispersion in [X/H] is consistent with the measurement errors, implying that the close comoving/wide binaries pairs are chemically homogeneous at our measurement precision.

We demonstrate that the far comoving pairs with separations of $2 \times 10^5 - 10^7$ AU also exhibit substantial chemical homogeneity (0.09 dex in the [Fe/H] scatter) compared to random pairs (0.23 dex). Nonetheless, the far comoving pairs less homogeneous than the close comoving/wide binaries population. If we assume that the far comoving pairs

comprise of a mixture of the conatal and random chance alignments population, modeling the distribution of Δ[Fe/H] as a mixture of these two populations implies that about $73 \pm 22\%$ of the unbound comoving stars with separations $2 \times 10^5 - 10^7$ AU and $\Delta v_{3D} < 2$ km s^{-1} are conatal. This conatality fraction is in excellent agreement with the predictions from simulations from Kamdar et al. (2019a).

Our study implies that most comoving stars are conatal, even though they are well-separated. As well-separated pairs of stars are more common than wide binaries, this new population of "clusters of two" enables many windows for studies that we have thus far restricted to the wide binaries and open clusters. Harnessing these vastly abundant comoving pairs will have broad applications, ranging from calibrating surveys to understanding star formation, planet engulfments, and beyond.

7. ACKNOWLEDGEMENTS

TN & KH have been partially supported by a TDA/Scialog (2018-2020) grant funded by the Research Corporation and a TDA/Scialog grant (2019-2021) funded by the Heising-Simons Foundation. TN & KH acknowledge support from the National Science Foundation grant AST-1907417. YST is grateful to be supported by the NASA Hubble Fellowship grant HST-HF2-51425.001 awarded by the Space Telescope Science Institute. KH is partially supported through the Wootton Center for Astrophysical Plasma Properties funded under the United States Department of Energy collaborative agreement DE-NA0003843. APJ acknowledges support from a Carnegie Fellowship and the Thacher Research Award in Astronomy. HK acknowledges support from the DOE CSGF under grant number DE-FG02-97ER25308. The authors thank Carnegie Observatory for granting us the observing time to conduct this study.

This research has made use of the SIMBAD database, operated at CDS, Strasbourg, France (Wenger et al. 2000) and NASA's Astrophysics Data System Bibliographic Services. This work has made use of data from the European Space Agency mission *Gaia* (https://www.cosmos.esa.int/gaia), processed by the Gaia Data Processing and Analysis Consortium (DPAC, https://www.cosmos.esa.int/web/gaia/dpac/consortium). Funding for the DPAC has been provided by national institutions, in particular the institutions participating in the Gaia Multilateral Agreement.

Facilities: Magellan/Clay Telescope, Simbad

Software: `astropy` (Astropy Collaboration et al. 2013, 2018), `NumPy` (Harris et al. 2020), `iPython` (Perez & Granger 2007), `Matplotlib` (Hunter 2007), `Galpy` (Bovy 2015), `SciPy` (Virtanen et al. 2020), `Photutils` (Bradley et al. 2020), `BACCHUS` (Masseron et al. 2016), `CarPy` (Kelson 2003), `topcat` (Taylor 2005), `iSpec` (Blanco-Cuaresma et al. 2014a)

Table 7. Atomic Data References

Reference Key	Reference
1968PhFl...11.1002W	Wolnik et al. (1968)
1969AA.....2..274G	Garz & Kock (1969)
1970AA.....9...37R	Richter & Wulff (1970)
1970ApJ...162.1037W	Wolnik et al. (1970)
1980AA....84..361B	Biemont & Godefroid (1980)
1980ZPhyA.298..249K	Kerkhoff et al. (1980)
1982ApJ...260..395C	Cardon et al. (1982)
1982MNRAS.199...21B	Blackwell et al. (1982a)
1983MNRAS.204..883B	Blackwell et al. (1983)
1984MNRAS.207..533B	Blackwell et al. (1984)
1984MNRAS.208..147B	Booth et al. (1984)
1984PhST....8...84K	Kock et al. (1984)
1985AA...153..109W	Whaling et al. (1985)
1985JQSRT..33..307D	Doerr & Kock (1985)
1986JQSRT..35..281D	Duquette et al. (1986)
1986MNRAS.220..289B	Blackwell et al. (1986a)
1989AA...208..157G	Grevesse et al. (1989)
1989ZPhyD..11..287C	Carlsson et al. (1989)
1990JQSRT..43..207C	Chang & Tang (1990)
1991JPhB...24.3943H	Hibbert et al. (1991)
1992AA...255..457D	Davidson et al. (1992)
1993AAS...99..179H	Hibbert et al. (1993)
1993JPhB...26.4409B	Butler et al. (1993)
1993PhyS...48..297N	Nahar (1993)
1995JPhB...28.3485M	Mendoza et al. (1995)
1996PhRvL..76.2862V	Volz et al. (1996)
1998PhRvA..57.1652Y	Yan et al. (1998)
1999ApJS..122..557N	Nitz et al. (1999)
2000MNRAS.312..813S	Storey & Zeippen (2000)
2003ApJ...584L.107J	Johansson et al. (2003)
2006JPCRD..35.1669F	Fuhr & Wiese (2006)
2006JPhB...39.2861Z	Zatsarinny & Bartschat (2006)
2007AA...472L..43B	Blackwell-Whitehead & Bergemann (2007)
2007PhyS...76..577L	Li et al. (2007)
2009A2009AA...497..611M	Meléndez & Barbuy (2009)
2009JPhB...42r5002K	Kułaga-Egger & Migdałek (2009)
2013ApJS..205...11L	Lawler et al. (2013a)
2013ApJS..208...27W	Wood et al. (2013a)

Table 7 *continued*

Table 7 *(continued)*

Reference Key	Reference
2014ApJS..211...20W	Wood et al. (2014)
2014MNRAS.441.3127R	Ruffoni et al. (2014)
ABH	Arnesen et al. (1977)
AMS	Andersen et al. (1972)
AMb	Alonso-Medina (1997)
APH	Andersen et al. (1976)
APR	Andersen et al. (1975)
AS	Andersen & Soerensen (1973)
ASa	Andersen & Sorensen (1974)
ASb	Anisimova & Semenov (1974)
ATJL	Aldenius et al. (2007)
Astrophysical	Kurucz (2007, 2009)[8]
BBC	Blanco et al. (1995)
BBEHL	Biémont et al. (2011)
BDMQ	Biémont et al. (1998)
BGF	Biemont et al. (1989)
BGHL	Biemont et al. (1981a)
BGHR	Baschek et al. (1970)
BGKZ	Biemont et al. (1984)
BHN	Bizzarri et al. (1993)
BIEMa	Biémont (1973)
BIEMb	Bièmont (1977)
BIPS	Blackwell et al. (1979a)
BK	Bard & Kock (1994)
BKK	Bard et al. (1991)
BKM	Biemont et al. (1982)
BKP,BKM	Blagoev et al. (1977); Biemont et al. (1982)
BKPb	Blagoev et al. (1978)
BKor	Bridges & Kornblith (1974)
BL	O'brian & Lawler (1991)
BLNP	Blackwell-Whitehead et al. (2006)
BLQS	Biémont et al. (2003)
BQR	Biémont et al. (2002)
BQZ	Biemont et al. (1993)
BRD	Biemont et al. (1981b)
BSB	Berzinsh et al. (1997)
BSScor	Blackwell et al. (1980)
BWL	O'Brian et al. (1991)

Table 7 *continued*

[8] There are four lines with this designation. Two Fe lines and two V lines. The Fe lines come from Kurucz (2007) and the V lines from Kurucz (2009). The loggf values were astrophysically calibrated.

Table 7 *(continued)*

Reference Key	Reference
BWL,BK	O'Brian et al. (1991); Bard & Kock (1994)
BXPNL	Blackwell-Whitehead et al. (2005)
Bar,BBC	Barach (1970); Blanco et al. (1995)
CB	Corliss & Bozman (1962a)
CBcor	Corliss & Bozman (1962b)
CC	Cowley & Corliss (1983a)
CCout	Cowley & Corliss (1983b)
CM	Clawson & Miller (1973)
CRC	Cowley (1973)
CSE	Cocke et al. (1973)
DCWL	den Hartog et al. (1998)
DHL	Den Hartog et al. (2005)
DHWL	Den Hartog et al. (2002)
DIKH	Drozdowski et al. (1997)
DLSC	Den Hartog et al. (2006)
DLSSC	Den Hartog et al. (2011)
DLW	Dolk et al. (2002)
DLa	Duquette & Lawler (1982)
DLb	Duquette & Lawler (1985)
DSJ	Dworetsky et al. (1984)
DSLa	Duquette et al. (1981)
DSLb	Duquette et al. (1982a)
DSLc	Duquette et al. (1982b)
ESTM	Kurucz (1993a)
FDLP	Fedchak et al. (2000)
FMW	Fuhr et al. (1988)
GARZ	Garz (1973)
GC	García & Campos (1988)
GESB79b	Blackwell et al. (1979b)
GESB82c	Blackwell et al. (1982b)
GESB82d	Blackwell et al. (1982c)
GESB86	Blackwell et al. (1986b)
GESG12	Grevesse (2012)
GESHRL14	Den Hartog et al. (2014)
GESMCHF	Froese Fischer & Tachiev (2012)
GESOP	Saraph & Storey (2012)
GHLa	Gough et al. (1982)
GHR	von der Goltz et al. (1984)
GHcor	Kurucz (1993b)
GKOPK	Gorshkov et al. (1980)
GKOa	Gorshkov et al. (1981)
GKOb	Gorshkov et al. (1983)

Table 7 *continued*

Table 7 *(continued)*

Reference Key	Reference
GNEL	Gurell et al. (2010)
GUES	Kurucz (1993c)
HLB	Hannaford et al. (1985)
HLGBW	Hannaford et al. (1982)
HLGN	Hannaford et al. (1992)
HLL	Hannaford et al. (1981)
HLSC	Den Hartog et al. (2003)
IAN	Ivarsson et al. (2003)
ILW	Ivarsson et al. (2001)
JMG	Migdalek (1978)
K03	Kurucz (2003)
K04	Kurucz (2004)
K06	Kurucz (2006)
K07	Kurucz (2007)
K08	Kurucz (2008)
K09	Kurucz (2009)
K10	Kurucz (2010)
K11	Kurucz (2011)
K12	Kurucz (2012)
K13	Kurucz (2013)
K14	Kurucz (2014)
K75	Kurucz (1975)
K99	Kurucz (1999)
KG	Kling & Griesmann (2000)
KK	Kroll & Kock (1987)
KP	Kurucz & Peytremann (1975)
KR	Kock & Richter (1968)
KSG	Kling et al. (2001)
KZB	Kwiatkowski et al. (1984)
KZBa	Kwiatkowski et al. (1982)
LAW	Lawrence (1967)
LBS	Lawler et al. (2001a)
LCG	Lotrian et al. (1978)
LCV	Laughlin et al. (1978)
LD	Lawler & Dakin (1989)
LD-HS	Lawler et al. (2006)
LDLS	Lawler et al. (2007)
LGWSC	Lawler et al. (2013b)
LGb	Lotrian & Guern (1982)
LMW	Lambert et al. (1969)
LN	Lindgård & Nielson (1977)
LNAJ	Ljung et al. (2006)

Table 7 *continued*

Table 7 *(continued)*

Reference Key	Reference
LNWLX	Lundqvist et al. (2006)
LSC	Lawler et al. (2004)
LSCI	Lawler et al. (2009)
LSCW	Lawler et al. (2008)
LV	Laughlin & Victor (1974)
LWCS	Lawler et al. (2001b)
LWG	Lawler et al. (1990)
LWHS	Lawler et al. (2001c)
LWST	Lennard et al. (1975)
LWa	Lambert & Warner (1968)
MC	Meggers et al. (1975)
MFW	Martin et al. (1988)
MIGa	Migdalek (1976)
MIGb	Migdałek (1976)
MRB	Miller et al. (1971)
MRW	May et al. (1974)
MULT	Kurucz (1993d)
MW	Miles & Wiese (1969)
MWRB	Miller et al. (1974)
NG	Grevesse (1969)
NHEL	Nilsson et al. (2010)
NI	Nilsson & Ivarsson (2008)
NIJL	Nilsson et al. (2002a)
NIST10	Ralchenko et al. (2010)
NWL	Nitz et al. (1998)
NZL	Nilsson et al. (2002b)
OK	Obbarius & Kock (1982)
PGBH	Pinnington et al. (1993)
PGHcor	Pauls et al. (1990)
PGK	Penkin et al. (1984)
PK	Penkin & Komarovskii (1976)
PN	Pitts & Newsom (1986)
PQB	Palmeri et al. (2001)
PQWB	Palmeri et al. (2000)
PRT	Parkinson et al. (1976)
PST	Pfennig et al. (1965)
PSa	Penkin & Shabanova (1963)
PTP	Pickering et al. (2001)
PV	Plekhotkin & Verolainen (1985)
QPB	Quinet et al. (1999a)
QPBM	Quinet et al. (1999b)
RHL	Ryabchikova et al. (1994)

Table 7 *continued*

Table 7 *(continued)*

Reference Key	Reference
RPU	Raassen et al. (1998)
RSa	Ryabchikova & Smirnov (1989)
RU	Raassen & Uylings (1998)
RW	Rosberg & Wyart (1997)
S	Smith (1988)
S-G,BBC	Schulz-Gulde (1969); Blanco et al. (1995)
SCRJ	Sansonetti & Reader (2001)
SDL	Salih et al. (1983)
SDcor	Schnehage et al. (1983)
SEN	Sengupta (1975)
SG	Smith & Gallagher (1966)
SK	Smith & Kuehne (1978)
SLS	Sobeck et al. (2007)
SLb	Salih & Lawler (1985)
SLd	Sigut & Landstreet (1990)
SN	Smith & O'Neill (1975)
SPN	Sikström et al. (2001)
SR	Smith & Raggett (1981)
Si2-av1	Ryabchikova (2012)
Sm	Smith (1981)
T	Theodosiou (1989)
T83av	Ryabchikova et al. (1999)
TB	Seaton et al. (1994)
VGH	Vaeck et al. (1988)
WBW	Wolnik et al. (1971)
WBb	Whaling & Brault (1988)
WGTG	Werij et al. (1992)
WL	Wickliffe & Lawler (1997a)
WLN	Wickliffe et al. (2000)
WLSC	Wood et al. (2013b)
WLa	Wickliffe & Lawler (1997b)
WM	Wiese & Martin (1980)
WSG	Wiese et al. (1966)
WSL	Wickliffe et al. (1994)
WSM	Wiese et al. (1969)
WV	Ward et al. (1985)
Wa	Warner (1968a)
Wc	Warner (1968b)
XJZD	Xu et al. (2003a)
XSCL	Xu et al. (2003b)
XSQG	Xu et al. (2003c)
ZLLZ	Zhiguo et al. (2000)

Table 7 *continued*

Table 7 *(continued)*

Reference Key	Reference
ZZZ	Zhiguo et al. (1999)

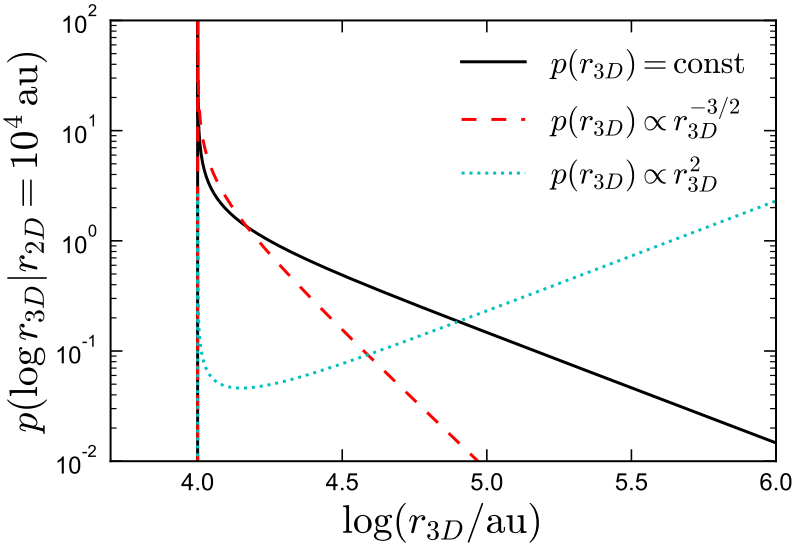

Figure 9. Conditional probability distribution of the logarithmic 3D separation r_{3D}, given a measured projected separation of $r_{2D} = 10^4$ AU. We compare distribution for three different choices of the prior on the intrinsic 3D separation distribution, $p(r_{3D})$. Dashed red line shows the prior we adopt for pairs suspected to be wide binaries. For both this choice and a flat prior (black line), $p\left(\log r_{3D}|r_{2D}\right)$ is sharply peaked at r_{2D}; that is, the most likely 3D separation is within a factor of a few of the projected separation. Dotted cyan line shows $p(r_{3D}) \propto r_{3D}^2$, as is expected for random chance alignments. In this case, the probability mass is dominated by pairs with $r_{3D} \gg r_{2D}$; that is, widely separated pairs viewed almost end-on.

APPENDIX

A. ESTIMATING 3D SEPARATIONS FOR WIDE BINARIES

Consider a pair of stars with true 3D separation r_{3D}. If the pair is viewed along a random viewing angle, the probability distribution of its projected separation r_{2D} can be calculated via a straightforward geometric argument (e.g. Nottale & Chamaraux 2018):

$$p\left(r_{2D}|r_{3D}\right) = \frac{1}{r_{3D}} \frac{r_{2D}/r_{3D}}{\sqrt{1-\left(r_{2D}/r_{3D}\right)^2}}. \tag{A1}$$

For the pairs in our sample suspected to be binaries, we have a precise measurement of r_{2D} and wish to constrain r_{3D}. By Bayes' rule, the probability distribution of r_{3D} given a measurement or r_{2D} depends both on the measured r_{2D}, and on the prior on r_{3D}.

$$p\left(r_{3D}|r_{2D}\right) \propto p\left(r_{2D}|r_{3D}\right) p\left(r_{3D}\right). \tag{A2}$$

The separation distribution of wide binaries is well-constrained observationally to be $p\left(r_{3D}\right) \sim r_{3D}^{-3/2}$ at $r_{3D} > 500$ AU (e.g. Andrews et al. 2017; El-Badry & Rix 2018), so we adopt this as the prior for the 3D separation distribution of pairs thought to be binaries. In this case, Equation A2 becomes

$$p\left(r_{3D}|r_{2D}\right) = \begin{cases} \frac{2}{\sqrt{\pi}} \frac{\Gamma(7/4)}{\Gamma(5/4)} \frac{1}{r_{3D}} \frac{\left(r_{2D}/r_{3D}\right)^{5/2}}{\sqrt{1-\left(r_{2D}/r_{3D}\right)^2}}, & r_{3D} > r_{2D} \\ 0 & \text{otherwise} \end{cases}, \tag{A3}$$

where Γ represents the Gamma function, and the coefficient is derived from the normalization condition. The red line in Figure 9 shows this distribution, with $r_{2D} = 10^4$ AU adopted for concreteness.[9] For this distribution, the median value of r_{3D}/r_{2D} is 1.12,

[9] For better visual interpretability, we plot $p\left(\log r_{3D}|r_{2D}\right) = \ln 10 \times r_{3D} \times p\left(r_{3D}|r_{2D}\right)$.

and the middle 68.2% range is (1.01, 1.61). Given a measurement of $r_{\rm 2D}$, we thus report $r_{\rm 3D} = 1.12^{+0.49}_{-0.11} \times r_{\rm 2D}$ if the pair is suspected to be a binary.

Of course, other choices are possible for the prior $p(r_{\rm 3D})$ when the separation exceeds what we expect from the binary population. The black line in Figure 9 corresponds to a "flat" prior, $p(r_{\rm 3D}) = {\rm const}$. Such a separation distribution might be expected for conatal pairs that are no longer bound, if the birth and dissolution rates of such pairs are constant. In this case, the median and 1σ range in $r_{\rm 3D}$ would be $r_{\rm 3D} = 1.41^{+2.63}_{-0.38} \times r_{\rm 2D}$, still implying that most pairs have 3D separations within a factor of a few of their 2D projected separation.

Finally, the dotted cyan line in Figure 9 shows the results of assuming $p(r_{\rm 3D}) \propto r_{\rm 3D}^2$. This is the distribution expected for random pairings of isotropically distributed stars. In this case, the probability distribution is normalizable only if we assume that there are no pairs beyond a 3D separation $r_{\rm max}$. The conditional probability distribution in this case is

$$p\left(r_{\rm 3D}|r_{\rm 2D}\right) = \begin{cases} \frac{1}{\sqrt{\left(1-r_{\rm 2D}^2/r_{\rm 3D}^2\right)\left(r_{\rm max}^2-r_{\rm 2D}^2\right)}}, & r_{\rm 3D} > r_{\rm 2D} \\ 0 & \text{otherwise} \end{cases}, \tag{A4}$$

which approaches a constant value at $r_{\rm 3D} \gg r_{\rm 2D}$. Intuitively, what happens in this case is that the larger number of possible pairs at large $r_{\rm 3D}$ (which scales as $r_{\rm 3D}^2$) exactly compensates for the smaller number of sightlines along which a pair can be viewed to have a given projected separation (which scales as $r_{\rm 3D}^{-2}$). In Figure 9, we adopt $r_{\rm max} = 10^6$ AU.

To summarize, we calculate constraints on the 3D separation of pairs thought to be wide binaries based on their projected 2D separation using Equation A3. This yields a median and 1σ range of $r_{\rm 3D} = 1.12^{+0.49}_{-0.11} \times r_{\rm 2D}$, which at small $r_{\rm 2D}$ is much more constraining than the constraint on $r_{\rm 3D}$ that considers the distances to both stars independently ("method 1"). The primary assumption of this constraint is that the separation distribution of wide binaries falls off as $p(r_{\rm 3D}) \propto r_{\rm 3D}^{-3/2}$. It is not appropriate for pairs that are not binaries (unbound comoving pairs or chance alignments), because their separation distribution is expect to *increase* with separation due to the different priors. We thus only apply this correction to pairs with separation $< 2 \times 10^5$ AU.

B. LINE LIST REFERENCES

A large part of this work is made possible by numerous heroic efforts by various groups who perform the pain-stacking tasks of curating/calibrating the atomic line list used in BACCHUS. Those efforts are unfortunately under appreciated in the literature. As such, albeit long, we decide to include the references to all original sources of the line list adopted in this study in Table 7.

REFERENCES

Aldenius, M., Tanner, J. D., Johansson, S., Lundberg, H., & Ryan, S. G. 2007, Astron. and Astrophys., 461, 767, doi: 10.1051/0004-6361:20066266

Alonso-Medina, A. 1997, PhyS, 55, 49, doi: 10.1088/0031-8949/55/1/008

Andersen, T., Madsen, O., & Sørensen, G. 1972, J. Opt. Soc. Am., 62, 1118, doi: 10.1364/JOSA.62.001118

Andersen, T., Petersen, P., & Hauge, O. 1976, SoPh, 49, 211, doi: 10.1007/BF00162445

Andersen, T., Poulsen, O., Ramanujam, P. S., & Petkov, A. P. 1975, SoPh, 44, 257, doi: 10.1007/BF00153206

Andersen, T., & Soerensen, G. 1973, JQSRT, 13, 369, doi: 10.1016/0022-4073(73)90066-6

Andersen, T., & Sorensen, G. 1974, SoPh, 38, 343, doi: 10.1007/BF00155072

Andrews, J. J., Agüeros, M. A., Gianninas, A., et al. 2015, ApJ, 815, 63, doi: 10.1088/0004-637X/815/1/63

Andrews, J. J., Anguiano, B., Chanamé, J., et al. 2019, ApJ, 871, 42, doi: 10.3847/1538-4357/aaf502

Andrews, J. J., Chanamé, J., & Agüeros, M. A. 2017, MNRAS, 472, 675, doi: 10.1093/mnras/stx2000

Anisimova, G. P., & Semenov, R. I. 1974, Optics and Spectroscopy, 36, 221

Arnesen, A., Bengtsson, A., Hallin, R., et al. 1977, PhyS, 16, 31, doi: 10.1088/0031-8949/16/1-2/004

Astropy Collaboration, Robitaille, T. P., Tollerud, E. J., et al. 2013, A&A, 558, A33, doi: 10.1051/0004-6361/201322068

Astropy Collaboration, Price-Whelan, A. M., Sipőcz, B. M., et al. 2018, AJ, 156, 123, doi: 10.3847/1538-3881/aabc4f

Barach, J. P. 1970, JQSRT, 10, 519, doi: 10.1016/0022-4073(70)90114-7

Bard, A., Kock, A., & Kock, M. 1991, Astron. and Astrophys., 248, 315

Bard, A., & Kock, M. 1994, Astron. and Astrophys., 282, 1014

Baschek, B., Garz, T., Holweger, H., & Richter, J. 1970, Astron. and Astrophys., 4, 229

Bernstein, R., Shectman, S. A., Gunnels, S. M., Mochnacki, S., & Athey, A. E. 2003, in Society of Photo-Optical Instrumentation Engineers (SPIE) Conference Series, Vol. 4841, Instrument Design and Performance for Optical/Infrared Ground-based Telescopes, ed. M. Iye & A. F. M. Moorwood, 1694–1704, doi: 10.1117/12.461502

Berzinsh, U., Svanberg, S., & Biemont, E. 1997, A&A, 326, 412

Biémont, E. 1973, Bulletin de la Societe Royale des Sciences de Liege, 42, 206

Bièmont, E. 1977, A&AS, 27, 489

Biémont, E., Dutrieux, J., Martin, I., & Quinet, P. 1998, Journal of Physics B Atomic Molecular Physics, 31, 3321, doi: 10.1088/0953-4075/31/15/006

Biemont, E., & Godefroid, M. 1980, A&A, 84, 361

Biemont, E., Grevesse, N., Faires, L. M., Marsden, G., & Lawler, J. E. 1989, A&A, 209, 391

Biemont, E., Grevesse, N., Hannaford, P., & Lowe, R. M. 1981a, ApJ, 248, 867, doi: 10.1086/159213

Biemont, E., Grevesse, N., Kwiatkovski, M., & Zimmermann, P. 1984, A&A, 131, 364

Biemont, E., Karner, C., Meyer, G., Traeger, F., & Zu Putlitz, G. 1982, A&A, 107, 166

Biémont, E., Lefèbvre, P., Quinet, P., Svanberg, S., & Xu, H. L. 2003, European Physical Journal D, 27, 33, doi: 10.1140/epjd/e2003-00235-1

Biémont, E., Quinet, P., & Ryabchikova, T. A. 2002, Monthly Notices Roy. Astron. Soc., 336, 1155, doi: 10.1046/j.1365-8711.2002.05868.x

Biemont, E., Quinet, P., & Zeippen, C. J. 1993, A&AS, 102, 435

Biemont, E., Roland, G., & Delbouille, L. 1981b, SoPh, 71, 223, doi: 10.1007/BF00167546

Biémont, É., Blagoev, K., Engström, L., et al. 2011, MNRAS, 414, 3350, doi: 10.1111/j.1365-2966.2011.18637.x

Bizzarri, A., Huber, M. C. E., Noels, A., et al. 1993, A&A, 273, 707

Blackwell, D. E., Booth, A. J., Menon, S. L. R., & Petford, A. D. 1986a, MNRAS, 220, 289, doi: 10.1093/mnras/220.2.289

—. 1986b, MNRAS, 220, 289

Blackwell, D. E., Ibbetson, P. A., Petford, A. D., & Shallis, M. J. 1979a, MNRAS, 186, 633

Blackwell, D. E., Menon, S. L. R., & Petford, A. D. 1983, MNRAS, 204, 883

—. 1984, MNRAS, 207, 533

Blackwell, D. E., Petford, A. D., & Shallis, M. J. 1979b, MNRAS, 186, 657

Blackwell, D. E., Petford, A. D., Shallis, M. J., & Leggett, S. 1982a, MNRAS, 199, 21

Blackwell, D. E., Petford, A. D., Shallis, M. J., & Simmons, G. J. 1982b, MNRAS, 199, 43

Blackwell, D. E., Petford, A. D., & Simmons, G. J. 1982c, MNRAS, 201, 595

Blackwell, D. E., Shallis, M. J., & Simmons, G. J. 1980, Astron. and Astrophys., 81, 340

Blackwell-Whitehead, R., & Bergemann, M. 2007, A&A, 472, L43, doi: 10.1051/0004-6361:20078165

Blackwell-Whitehead, R. J., Lundberg, H., Nave, G., et al. 2006, Monthly Notices Roy. Astron. Soc., 373, 1603, doi: 10.1111/j.1365-2966.2006.11161.x

Blackwell-Whitehead, R. J., Xu, H. L., Pickering, J. C., Nave, G., & Lundberg, H. 2005, MNRAS, 361, 1281, doi: 10.1111/j.1365-2966.2005.09264.x

Blagoev, K. B., Komarovskii, V. A., & Penkin, N. P. 1977, Optics and Spectroscopy, 42, 238

—. 1978, Optics and Spectroscopy, 44, 131

Blanco, F., Botho, B., & Campos, J. 1995, PhyS, 52, 628, doi: 10.1088/0031-8949/52/6/004

Blanco-Cuaresma, S., Soubiran, C., Heiter, U., & Jofré, P. 2014a, A&A, 569, A111, doi: 10.1051/0004-6361/201423945

Blanco-Cuaresma, S., Soubiran, C., Jofré, P., & Heiter, U. 2014b, A&A, 566, A98, doi: 10.1051/0004-6361/201323153

Booth, A. J., Blackwell, D. E., Petford, A. D., & Shallis, M. J. 1984, MNRAS, 208, 147

Booth, R. S., Poppenhaeger, K., Watson, C. A., Silva Aguirre, V., & Wolk, S. J. 2017, MNRAS, 471, 1012, doi: 10.1093/mnras/stx1630

Bovy, J. 2015, ApJS, 216, 29, doi: 10.1088/0067-0049/216/2/29

Bradley, L., Sipőcz, B., Robitaille, T., et al. 2020, astropy/photutils: 1.0.0, 1.0.0, Zenodo, doi: 10.5281/zenodo.4044744

Bridges, J. M., & Kornblith, R. L. 1974, ApJ, 192, 793, doi: 10.1086/153118

Butler, K., Mendoza, C., & Zeippen, C. J. 1993, Journal of Physics B Atomic Molecular Physics, 26, 4409, doi: 10.1088/0953-4075/26/23/013

Cantat-Gaudin, T., & Anders, F. 2020, A&A, 633, A99, doi: 10.1051/0004-6361/201936691

Cardon, B. L., Smith, P. L., Scalo, J. M., Testerman, L., & Whaling, W. 1982, ApJ, 260, 395, doi: 10.1086/160264

Carlsson, J., Sturesson, L., & Svanberg, S. 1989, Zeitschrift fur Physik D Atoms Molecules Clusters, 11, 287, doi: 10.1007/BF01438501

Chang, T. N., & Tang, X. 1990, JQSRT, 43, 207, doi: 10.1016/0022-4073(90)90053-9

Clawson, J. E., & Miller, M. H. 1973, Journal of the Optical Society of America (1917-1983), 63, 1598

Cocke, C. L., Stark, A., & Evans, J. C. 1973, ApJ, 184, 653, doi: 10.1086/152357

Corliss, C. H., & Bozman, W. R. 1962a, NBS Monograph, Vol. 53, Experimental transition probabilities for spectral lines of seventy elements; derived from the NBS Tables of spectral-line intensities, ed. Corliss, C. H. & Bozman, W. R. (US Government Printing Office)

—. 1962b, NBS Monograph, Vol. 53, Experimental transition probabilities for spectral lines of seventy elements; derived from the NBS Tables of spectral-line intensities, ed. Corliss, C. H. & Bozman, W. R. (Washington DC: US Government Printing Office)

Cowley, C. R. 1973, Journ. Res. NBS, 77A, 419

Cowley, C. R., & Corliss, C. H. 1983a, MNRAS, 203, 651

—. 1983b, MNRAS, 203, 651

Davidson, M. D., Snoek, L. C., Volten, H., & Doenszelmann, A. 1992, A&A, 255, 457

De Silva, G. M., Freeman, K. C., Asplund, M., et al. 2007, AJ, 133, 1161, doi: 10.1086/511182

den Hartog, E. A., Curry, J. J., Wickliffe, M. E., & Lawler, J. E. 1998, SoPh, 178, 239

Den Hartog, E. A., Herd, M. T., Lawler, J. E., et al. 2005, Astrophys. J., 619, 639, doi: 10.1086/426381

Den Hartog, E. A., Lawler, J. E., Sneden, C., & Cowan, J. J. 2003, Astrophys. J. Suppl. Ser., 148, 543, doi: 10.1086/376940

—. 2006, Astrophys. J. Suppl. Ser., 167, 292, doi: 10.1086/508262

Den Hartog, E. A., Lawler, J. E., Sobeck, J. S., Sneden, C., & Cowan, J. J. 2011, ApJS, 194, 35, doi: 10.1088/0067-0049/194/2/35

Den Hartog, E. A., Ruffoni, M. P., Lawler, J. E., et al. 2014, ArXiv e-prints. https://arxiv.org/abs/1409.8142

Den Hartog, E. A., Wickliffe, M. E., & Lawler, J. E. 2002, Astrophys. J. Suppl. Ser., 141, 255, doi: 10.1086/340039

Doerr, A., & Kock, M. 1985, JQSRT, 33, 307, doi: 10.1016/0022-4073(85)90192-X

Dolk, L., Litzén, U., & Wahlgren, G. M. 2002, Astron. and Astrophys., 388, 692, doi: 10.1051/0004-6361:20020573

Dotter, A., Conroy, C., Cargile, P., & Asplund, M. 2017, ApJ, 840, 99, doi: 10.3847/1538-4357/aa6d10

Drozdowski, R., Ignaciuk, M., Kwela, J., & Heldt, J. 1997, Zeitschrift fur Physik D Atoms Molecules Clusters, 41, 125, doi: 10.1007/s004600050300

Duquette, D. W., den Hartog, E. A., & Lawler, J. E. 1986, JQSRT, 35, 281, doi: 10.1016/0022-4073(86)90082-8

Duquette, D. W., & Lawler, J. E. 1982, PhRvA, 26, 330, doi: 10.1103/PhysRevA.26.330

—. 1985, Journal of the Optical Society of America B Optical Physics, 2, 1948, doi: 10.1364/JOSAB.2.001948

Duquette, D. W., Salih, S., & Lawler, J. E. 1981, PhRvA, 24, 2847, doi: 10.1103/PhysRevA.24.2847

—. 1982a, PhRvA, 26, 2623, doi: 10.1103/PhysRevA.26.2623

—. 1982b, Journal of Physics B Atomic Molecular Physics, 15, L897, doi: 10.1088/0022-3700/15/24/004

Dworetsky, M. M., Storey, P. J., & Jacobs, J. M. 1984, Physica Scripta Volume T, 8, 39, doi: 10.1088/0031-8949/1984/T8/006

El-Badry, K., & Rix, H.-W. 2018, MNRAS, 480, 4884, doi: 10.1093/mnras/sty2186

El-Badry, K., Rix, H.-W., & Heintz, T. M. 2021, arXiv e-prints, arXiv:2101.05282. https://arxiv.org/abs/2101.05282

El-Badry, K., Rix, H.-W., Ting, Y.-S., et al. 2018, MNRAS, 473, 5043, doi: 10.1093/mnras/stx2758

Fedchak, J. A., Den Hartog, E. A., Lawler, J. E., et al. 2000, Astrophys. J., 542, 1109, doi: 10.1086/317034

Feng, Y., & Krumholz, M. R. 2014, Nature, 513, 523, doi: 10.1038/nature13662

Froese Fischer, C., & Tachiev, G. 2012, Multiconfiguration Hartree-Fock and Multiconfiguration Dirac-Hartree-Fock Collection, Version 2, National Institute of Standards and Technology

Fuhr, J. R., Martin, G. A., & Wiese, W. L. 1988, Journal of Physical and Chemical Reference Data, Volume 17, Suppl. 4. New York: American Institute of Physics (AIP) and American Chemical Society, 1988, 17

Fuhr, J. R., & Wiese, W. L. 2006, Journal of Physical and Chemical Reference Data, 35, 1669, doi: 10.1063/1.2218876

Gaia Collaboration, Brown, A. G. A., Vallenari, A., et al. 2020, arXiv e-prints, arXiv:2012.01533. https://arxiv.org/abs/2012.01533

—. 2018, A&A, 616, A1, doi: 10.1051/0004-6361/201833051

Garcés, A., Catalán, S., & Ribas, I. 2011, A&A, 531, A7, doi: 10.1051/0004-6361/201116775

García, G., & Campos, J. 1988, JQSRT, 39, 477, doi: 10.1016/0022-4073(88)90093-3

García Pérez, A. E., Allende Prieto, C., Holtzman, J. A., et al. 2016, AJ, 151, 144, doi: 10.3847/0004-6256/151/6/144

Garz, T. 1973, A&A, 26, 471

Garz, T., & Kock, M. 1969, A&A, 2, 274

Gorshkov, V. N., Komarovskii, V. A., Oserovich, A. L., Penkin, N. P., & Khefferlin, R. 1980, Optics and Spectroscopy, 48, 362

Gorshkov, V. N., Komarovskii, V. A., Osherovich, A. L., & Penkin, N. P. 1981, Astrofizika, 17, 799

—. 1983, Optics and Spectroscopy, 54, 122

Gough, D. S., Hannaford, P., & Lowe, R. M. 1982, Journal of Physics B Atomic Molecular Physics, 15, L431, doi: 10.1088/0022-3700/15/13/003

Gray, D. F. 2008, The Observation and Analysis of Stellar Photospheres

Grevesse, N. 1969, SoPh, 6, 381, doi: 10.1007/BF00146472

—. 2012

Grevesse, N., Asplund, M., & Sauval, A. J. 2007, SSRv, 130, 105, doi: 10.1007/s11214-007-9173-7

Grevesse, N., Blackwell, D. E., & Petford, A. D. 1989, A&A, 208, 157
Gurell, J., Nilsson, H., Engström, L., et al. 2010, A&A, 511, A68+, doi: 10.1051/0004-6361/200913672
Gustafsson, B., Edvardsson, B., Eriksson, K., et al. 2008, A&A, 486, 951, doi: 10.1051/0004-6361:200809724
Hannaford, P., Larkins, P. L., & Lowe, R. M. 1981, Journal of Physics B Atomic Molecular Physics, 14, 2321, doi: 10.1088/0022-3700/14/14/004
Hannaford, P., Lowe, R. M., Biemont, E., & Grevesse, N. 1985, A&A, 143, 447
Hannaford, P., Lowe, R. M., Grevesse, N., Biemont, E., & Whaling, W. 1982, ApJ, 261, 736, doi: 10.1086/160384
Hannaford, P., Lowe, R. M., Grevesse, N., & Noels, A. 1992, Astron. and Astrophys., 259, 301
Harris, C. R., Millman, K. J., van der Walt, S. J., et al. 2020, Nature, 585, 357–362, doi: 10.1038/s41586-020-2649-2
Hawkins, K., Lucey, M., & Curtis, J. 2020a, MNRAS, 496, 2422, doi: 10.1093/mnras/staa1673
Hawkins, K., Kordopatis, G., Gilmore, G., et al. 2015, MNRAS, 447, 2046, doi: 10.1093/mnras/stu2574
Hawkins, K., Lucey, M., Ting, Y.-S., et al. 2020b, MNRAS, 492, 1164, doi: 10.1093/mnras/stz3132
Heiter, U., Jofré, P., Gustafsson, B., et al. 2015, A&A, 582, A49, doi: 10.1051/0004-6361/201526319
Heiter, U., Lind, K., Bergemann, M., et al. 2019, A&A
Hibbert, A., Biemont, E., Godefroid, M., & Vaeck, N. 1991, Journal of Physics B Atomic Molecular Physics, 24, 3943, doi: 10.1088/0953-4075/24/18/010
—. 1993, A&AS, 99, 179
Hunter, J. D. 2007, Computing in Science Engineering, 9, 90, doi: 10.1109/MCSE.2007.55
Ivarsson, S., Litzén, U., & Wahlgren, G. M. 2001, Physica Scripta, 64, 455, doi: 10.1238/Physica.Regular.064a00455
Ivarsson, S., Andersen, J., Nordström, B., et al. 2003, Astron. and Astrophys., 409, 1141, doi: 10.1051/0004-6361:20031184
Jiang, Y.-F., & Tremaine, S. 2010, MNRAS, 401, 977, doi: 10.1111/j.1365-2966.2009.15744.x
Jofré, P., Heiter, U., & Soubiran, C. 2019, ARA&A, 57, 571, doi: 10.1146/annurev-astro-091918-104509
Jofré, P., Heiter, U., Soubiran, C., et al. 2014, A&A, 564, A133, doi: 10.1051/0004-6361/201322440
Johansson, S., Litzén, U., Lundberg, H., & Zhang, Z. 2003, ApJL, 584, L107, doi: 10.1086/374037
Kamdar, H., Conroy, C., & Ting, Y.-S. 2021, arXiv e-prints, arXiv:2106.02050. https://arxiv.org/abs/2106.02050
Kamdar, H., Conroy, C., Ting, Y.-S., et al. 2019a, ApJ, 884, 173, doi: 10.3847/1538-4357/ab44be
—. 2019b, ApJL, 884, L42, doi: 10.3847/2041-8213/ab4997
Kelson, D. D. 2003, PASP, 115, 688, doi: 10.1086/375502
Kerkhoff, H., Schmidt, M., & Zimmermann, P. 1980, Zeitschrift fur Physik A Hadrons and Nuclei, 298, 249, doi: 10.1007/BF01425154
Kling, R., & Griesmann, U. 2000, ApJ, 531, 1173, doi: 10.1086/308490
Kling, R., Schnabel, R., & Griesmann, U. 2001, ApJS, 134, 173, doi: 10.1086/320366
Kock, M., Kroll, S., & Schnehage, S. 1984, Physica Scripta Volume T, 8, 84, doi: 10.1088/0031-8949/1984/T8/013
Kock, M., & Richter, J. 1968, ZA, 69, 180
Kounkel, M., & Covey, K. 2019, AJ, 158, 122, doi: 10.3847/1538-3881/ab339a
Kouwenhoven, M. B. N., Goodwin, S. P., Parker, R. J., et al. 2010, MNRAS, 404, 1835, doi: 10.1111/j.1365-2966.2010.16399.x
Kroll, S., & Kock, M. 1987, Astron. and Astrophys. Suppl. Ser., 67, 225
Kułaga-Egger, D., & Migdałek, J. 2009, Journal of Physics B Atomic Molecular Physics, 42, 185002, doi: 10.1088/0953-4075/42/18/185002
Kurucz, R. L. 1975
—. 1992, RMxAA, 23, 45
—. 1993a
—. 1993b
—. 1993c
—. 1993d
—. 1999, Robert L. Kurucz on-line database of observed and predicted atomic transitions
—. 2003, Robert L. Kurucz on-line database of observed and predicted atomic transitions
—. 2004, Robert L. Kurucz on-line database of observed and predicted atomic transitions
—. 2006, Robert L. Kurucz on-line database of observed and predicted atomic transitions
—. 2007, Robert L. Kurucz on-line database of observed and predicted atomic transitions
—. 2008, Robert L. Kurucz on-line database of observed and predicted atomic transitions
—. 2009, Robert L. Kurucz on-line database of observed and predicted atomic transitions
—. 2010, Robert L. Kurucz on-line database of observed and predicted atomic transitions
—. 2011, Robert L. Kurucz on-line database of observed and predicted atomic transitions
—. 2012, Robert L. Kurucz on-line database of observed and predicted atomic transitions
—. 2013, Robert L. Kurucz on-line database of observed and predicted atomic transitions
—. 2014, Robert L. Kurucz on-line database of observed and predicted atomic transitions
Kurucz, R. L., & Peytremann, E. 1975, SAO Special Report, 362, 1

Kwiatkowski, M., Zimmermann, P., Biemont, E., & Grevesse, N. 1982, A&A, 112, 337
—. 1984, Astron. and Astrophys., 135, 59
Lambert, D. L., Mallia, E. A., & Warner, B. 1969, MNRAS, 142, 71
Lambert, D. L., & Warner, B. 1968, MNRAS, 138, 181
Laughlin, C., Constantinides, E. R., & Victor, G. A. 1978, Journal of Physics B Atomic Molecular Physics, 11, 2243, doi: 10.1088/0022-3700/11/13/008
Laughlin, C., & Victor, G. A. 1974, ApJ, 192, 551, doi: 10.1086/153090
Lawler, J. E., Bonvallet, G., & Sneden, C. 2001a, Astrophys. J., 556, 452, doi: 10.1086/321549
Lawler, J. E., & Dakin, J. T. 1989, Journal of the Optical Society of America B Optical Physics, 6, 1457, doi: 10.1364/JOSAB.6.001457
Lawler, J. E., den Hartog, E. A., Labby, Z. E., et al. 2007, Astrophys. J. Suppl. Ser., 169, 120, doi: 10.1086/510368
Lawler, J. E., Den Hartog, E. A., Sneden, C., & Cowan, J. J. 2006, Astrophys. J. Suppl. Ser., 162, 227, doi: 10.1086/498213
Lawler, J. E., Guzman, A., Wood, M. P., Sneden, C., & Cowan, J. J. 2013a, ApJS, 205, 11, doi: 10.1088/0067-0049/205/2/11
—. 2013b, ApJS, 205, 11, doi: 10.1088/0067-0049/205/2/11
Lawler, J. E., Sneden, C., & Cowan, J. J. 2004, Astrophys. J., 604, 850, doi: 10.1086/382068
Lawler, J. E., Sneden, C., Cowan, J. J., Ivans, I. I., & Den Hartog, E. A. 2009, Astrophys. J. Suppl. Ser., 182, 51, doi: 10.1088/0067-0049/182/1/51
Lawler, J. E., Sneden, C., Cowan, J. J., et al. 2008, Astrophys. J. Suppl. Ser., 178, 71, doi: 10.1086/589834
Lawler, J. E., Whaling, W., & Grevesse, N. 1990, Nature, 346, 635, doi: 10.1038/346635a0
Lawler, J. E., Wickliffe, M. E., Cowley, C. R., & Sneden, C. 2001b, Astrophys. J. Suppl. Ser., 137, 341, doi: 10.1086/323001
Lawler, J. E., Wickliffe, M. E., den Hartog, E. A., & Sneden, C. 2001c, Astrophys. J., 563, 1075, doi: 10.1086/323407
Lawrence, G. M. 1967, ApJ, 148, 261, doi: 10.1086/149143
Lee, J.-E., Lee, S., Dunham, M. M., et al. 2017, Nature Astronomy, 1, 0172, doi: 10.1038/s41550-017-0172
Lennard, W. N., Whaling, W., Scalo, J. M., & Testerman, L. 1975, ApJ, 197, 517, doi: 10.1086/153538
Lépine, S., & Bongiorno, B. 2007, AJ, 133, 889, doi: 10.1086/510333
Li, R., Chatelain, R., Holt, R. A., et al. 2007, PhyS, 76, 577, doi: 10.1088/0031-8949/76/5/028
Lindgård, A., & Nielson, S. E. 1977, Atomic Data and Nuclear Data Tables, 19, 533, doi: 10.1016/0092-640X(77)90017-1
Liu, F., Asplund, M., Ramirez, I., Yong, D., & Melendez, J. 2014, MNRAS, 442, L51, doi: 10.1093/mnrasl/slu055
Ljung, G., Nilsson, H., Asplund, M., & Johansson, S. 2006, A&A, 456, 1181, doi: 10.1051/0004-6361:20065212
Lotrian, J., Cariou, J., Guern, Y., & Johannin-Gilles, A. 1978, Journal of Physics B Atomic Molecular Physics, 11, 2273, doi: 10.1088/0022-3700/11/13/011
Lotrian, J., & Guern, Y. 1982, Journal of Physics B Atomic Molecular Physics, 15, 69, doi: 10.1088/0022-3700/15/1/014
Lundqvist, M., Nilsson, H., Wahlgren, G. M., et al. 2006, Astron. and Astrophys., 450, 407, doi: 10.1051/0004-6361:20054474
Mack, Claude E., I., Schuler, S. C., Stassun, K. G., & Norris, J. 2014, ApJ, 787, 98, doi: 10.1088/0004-637X/787/2/98
Mack, Claude E., I., Stassun, K. G., Schuler, S. C., Hebb, L., & Pepper, J. A. 2016, ApJ, 818, 54, doi: 10.3847/0004-637X/818/1/54
Martin, G., Fuhr, J., & Wiese, W. 1988, J. Phys. Chem. Ref. Data Suppl., 17
Masseron, T., Merle, T., & Hawkins, K. 2016, BACCHUS: Brussels Automatic Code for Characterizing High accUracy Spectra, Astrophysics Source Code Library, doi: 10.20356/C4TG6R
Masseron, T., Plez, B., Van Eck, S., et al. 2014, A&A, 571, A47, doi: 10.1051/0004-6361/201423956
May, M., Richter, J., & Wichelmann, J. 1974, A&AS, 18, 405
Meggers, W. F., Corliss, C. H., & Scribner, B. F. 1975, Tables of spectral-line intensities. Part I, II_- arranged by elements., ed. Meggers, W. F., Corliss, C. H., & Scribner, B. F.
Meléndez, J., & Barbuy, B. 2009, A&A, 497, 611, doi: 10.1051/0004-6361/200811508
Meléndez, J., Bedell, M., Bean, J. L., et al. 2017, A&A, 597, A34, doi: 10.1051/0004-6361/201527775
Mendoza, C., Eissner, W., LeDourneuf, M., & Zeippen, C. J. 1995, Journal of Physics B Atomic Molecular Physics, 28, 3485, doi: 10.1088/0953-4075/28/16/006
Migdalek, J. 1976, JQSRT, 16, 265, doi: 10.1016/0022-4073(76)90068-6
Migdałek, J. 1976, Canadian Journal of Physics, 54, 2272
Migdalek, J. 1978, JQSRT, 20, 81, doi: 10.1016/0022-4073(78)90009-2
Miles, B. M., & Wiese, W. L. 1969, Atomic Data, 1, 1, doi: 10.1016/S0092-640X(69)80019-7
Miller, M. H., Roig, R. A., & Bengtson, R. D. 1971, PhRvA, 4, 1709, doi: 10.1103/PhysRevA.4.1709
Miller, M. H., Wilkerson, T. D., Roig, R. A., & Bengtson, R. D. 1974, PhRvA, 9, 2312, doi: 10.1103/PhysRevA.9.2312
Moeckel, N., & Clarke, C. J. 2011, MNRAS, 415, 1179, doi: 10.1111/j.1365-2966.2011.18731.x
Montes, D., González-Peinado, R., Tabernero, H. M., et al. 2018, MNRAS, 479, 1332, doi: 10.1093/mnras/sty1295
Nahar, S. N. 1993, PhyS, 48, 297, doi: 10.1088/0031-8949/48/3/008

Ness, M., Rix, H. W., Hogg, D. W., et al. 2018, ApJ, 853, 198, doi: 10.3847/1538-4357/aa9d8e
Nilsson, H., & Ivarsson, S. 2008, A&A, 492, 609, doi: 10.1051/0004-6361:200811019
Nilsson, H., Ivarsson, S., Johansson, S., & Lundberg, H. 2002a, Astron. and Astrophys., 381, 1090, doi: 10.1051/0004-6361:20011540
Nilsson, H., Zhang, Z. G., Lundberg, H., Johansson, S., & Nordström, B. 2002b, Astron. and Astrophys., 382, 368, doi: 10.1051/0004-6361:20011597
Nilsson, H., Hartman, H., Engström, L., et al. 2010, A&A, 511, A16+, doi: 10.1051/0004-6361/200913574
Nissen, P. E., & Gustafsson, B. 2018, A&A Rv, 26, 6, doi: 10.1007/s00159-018-0111-3
Nitz, D. E., Kunau, A. E., Wilson, K. L., & Lentz, L. R. 1999, ApJS, 122, 557, doi: 10.1086/313223
Nitz, D. E., Wickliffe, M. E., & Lawler, J. E. 1998, Astrophys. J. Suppl. Ser., 117, 313, doi: 10.1086/313112
Nottale, L., & Chamaraux, P. 2018, A&A, 614, A45, doi: 10.1051/0004-6361/201832707
Obbarius, H. U., & Kock, M. 1982, Journal of Physics B Atomic Molecular Physics, 15, 527, doi: 10.1088/0022-3700/15/4/006
O'brian, T. R., & Lawler, J. E. 1991, PhRvA, 44, 7134, doi: 10.1103/PhysRevA.44.7134
O'Brian, T. R., Wickliffe, M. E., Lawler, J. E., Whaling, W., & Brault, J. W. 1991, Journal of the Optical Society of America B Optical Physics, 8, 1185
Offner, S. S. R., Kratter, K. M., Matzner, C. D., Krumholz, M. R., & Klein, R. I. 2010, ApJ, 725, 1485, doi: 10.1088/0004-637X/725/2/1485
Oh, S., Price-Whelan, A. M., Brewer, J. M., et al. 2018, ApJ, 854, 138, doi: 10.3847/1538-4357/aaab4d
Oh, S., Price-Whelan, A. M., Hogg, D. W., Morton, T. D., & Spergel, D. N. 2017, AJ, 153, 257, doi: 10.3847/1538-3881/aa6ffd
Palmeri, P., Quinet, P., & Biémont, E. 2001, Physica Scripta, 63, 468, doi: 10.1238/Physica.Regular.063a00468
Palmeri, P., Quinet, P., Wyart, J., & Biémont, E. 2000, Physica Scripta, 61, 323, doi: 10.1238/Physica.Regular.061a00323
Parkinson, W. H., Reeves, E. M., & Tomkins, F. S. 1976, Royal Society of London Proceedings Series A, 351, 569, doi: 10.1098/rspa.1976.0157
Pauls, U., Grevesse, N., & Huber, M. C. E. 1990, Astron. and Astrophys., 231, 536
Penkin, N. P., Gorshkov, V. N., & Komarovskii, V. A. 1984, Optics and Spectroscopy, 57, 488
Penkin, N. P., & Komarovskii, V. A. 1976, JQSRT, 16, 217, doi: 10.1016/0022-4073(76)90066-2
Penkin, N. P., & Shabanova, L. N. 1963, Optics and Spectroscopy, 14, 5
Perez, F., & Granger, B. E. 2007, Computing in Science Engineering, 9, 21, doi: 10.1109/MCSE.2007.53
Pfennig, H., Steele, R., & Trefftz, E. 1965, JQSRT, 5, 335, doi: 10.1016/0022-4073(65)90070-1
Pickering, J. C., Thorne, A. P., & Perez, R. 2001, Astrophys. J. Suppl. Ser., 132, 403, doi: 10.1086/318958
Pinnington, E. H., Ji, Q., Guo, B., et al. 1993, Canadian Journal of Physics, 71, 470
Pitts, R. E., & Newsom, G. H. 1986, JQSRT, 35S, 383, doi: 10.1016/0022-4073(86)90024-5
Plekhotkin, G. A., & Verolainen, Y. F. 1985, Optics and Spectroscopy, 58, 447
Plez, B. 2012, Turbospectrum: Code for spectral synthesis. http://ascl.net/1205.004
Quinet, P., Palmeri, P., & Biemont, E. 1999a, J. Quant. Spectrosc. Radiat. Transfer, 62, 625, doi: 10.1016/S0022-4073(98)00127-7
Quinet, P., Palmeri, P., Biémont, E., et al. 1999b, Monthly Notices Roy. Astron. Soc., 307, 934, doi: 10.1046/j.1365-8711.1999.02689.x
Raassen, A. J. J., Pickering, J. C., & Uylings, P. H. M. 1998, A&AS, 130, 541, doi: 10.1051/aas:1998242
Raassen, A. J. J., & Uylings, P. H. M. 1998, A&A, 340, 300
Ralchenko, Y., Kramida, A., Reader, J., & NIST ASD Team. 2010, NIST Atomic Spectra Database (ver. 4.0.0), [Online]., National Institute of Standards and Technology, Gaithersburg, MD.
Ramírez, I., Asplund, M., Baumann, P., Meléndez, J., & Bensby, T. 2010, A&A, 521, A33, doi: 10.1051/0004-6361/201014456
Ramírez, I., Fish, J. R., Lambert, D. L., & Allende Prieto, C. 2012, ApJ, 756, 46, doi: 10.1088/0004-637X/756/1/46
Ramírez, I., Khanal, S., Lichon, S. J., et al. 2019, MNRAS, 490, 2448, doi: 10.1093/mnras/stz2709
Ramírez, I., Meléndez, J., Bean, J., et al. 2014, A&A, 572, A48, doi: 10.1051/0004-6361/201424244
Rebassa-Mansergas, A., Anguiano, B., García-Berro, E., et al. 2016, MNRAS, 463, 1137, doi: 10.1093/mnras/stw2021
Reggiani, H., & Meléndez, J. 2018, MNRAS, 475, 3502, doi: 10.1093/mnras/sty104
Reipurth, B., & Mikkola, S. 2012, Nature, 492, 221, doi: 10.1038/nature11662
Richter, J., & Wulff, P. 1970, A&A, 9, 37
Rojas-Ayala, B., Covey, K. R., Muirhead, P. S., & Lloyd, J. P. 2010, ApJL, 720, L113, doi: 10.1088/2041-8205/720/1/L113
Rosberg, M., & Wyart, J.-F. 1997, PhyS, 55, 690, doi: 10.1088/0031-8949/55/6/009
Ruchti, G. R., Bergemann, M., Serenelli, A., Casagrande, L., & Lind, K. 2013, MNRAS, 429, 126, doi: 10.1093/mnras/sts319
Ruffoni, M. P., Den Hartog, E. A., Lawler, J. E., et al. 2014, MNRAS, 441, 3127, doi: 10.1093/mnras/stu780
Ryabchikova, T. A. 2012

Ryabchikova, T. A., Hill, G. M., Landstreet, J. D., Piskunov, N., & Sigut, T. A. A. 1994, MNRAS, 267, 697
Ryabchikova, T. A., Piskunov, N. E., Stempels, H. C., Kupka, F., & Weiss, W. W. 1999, Physica Scripta Volume T, 83, 162, doi: 10.1238/Physica.Topical.083a00162
Ryabchikova, T. A., & Smirnov, Y. M. 1989, Astron. Tsirk., 21
Saffe, C., Flores, M., Jaque Arancibia, M., Buccino, A., & Jofré, E. 2016, A&A, 588, A81, doi: 10.1051/0004-6361/201528043
Saffe, C., Jofré, E., Martioli, E., et al. 2017, A&A, 604, L4, doi: 10.1051/0004-6361/201731430
Salih, S., Duquette, D. W., & Lawler, J. E. 1983, PhRvA, 27, 1193, doi: 10.1103/PhysRevA.27.1193
Salih, S., & Lawler, J. E. 1985, Journal of the Optical Society of America B Optical Physics, 2, 422, doi: 10.1364/JOSAB.2.000422
Sanders, N. E., Caldwell, N., McDowell, J., & Harding, P. 2012, ApJ, 758, 133, doi: 10.1088/0004-637X/758/2/133
Sansonetti, C. J., & Reader, J. 2001, Physica Scripta, 63, 219, doi: 10.1238/Physica.Regular.063a00219
Saraph, H., & Storey, P. 2012, The Opacity Project
Schnehage, S. E., Danzmann, K., Kuennemeyer, R., & Kock, M. 1983, JQSRT, 29, 507, doi: 10.1016/0022-4073(83)90127-9
Schuler, S. C., Cunha, K., Smith, V. V., et al. 2011, ApJL, 737, L32, doi: 10.1088/2041-8205/737/2/L32
Schulz-Gulde, E. 1969, JQSRT, 9, 13, doi: 10.1016/0022-4073(69)90144-7
Seaton, M. J., Yan, Y., Mihalas, D., & Pradhan, A. K. 1994, Monthly Notices Roy. Astron. Soc., 266, 805
Sengupta, S. 1975, JQSRT, 15, 159, doi: 10.1016/0022-4073(75)90014-X
Sigut, T. A. A., & Landstreet, J. D. 1990, MNRAS, 247, 611
Sikström, C. M., Pihlemark, H., Nilsson, H., et al. 2001, Journal of Physics B Atomic Molecular Physics, 34, 477, doi: 10.1088/0953-4075/34/3/323
Smiljanic, R., Korn, A. J., Bergemann, M., et al. 2014, A&A, 570, A122, doi: 10.1051/0004-6361/201423937
Smith, G. 1981, Astron. and Astrophys., 103, 351
—. 1988, Journal of Physics B Atomic Molecular Physics, 21, 2827, doi: 10.1088/0953-4075/21/16/008
Smith, G., & O'Neill, J. A. 1975, Astron. and Astrophys., 38, 1
Smith, G., & Raggett, D. S. J. 1981, Journal of Physics B Atomic Molecular Physics, 14, 4015, doi: 10.1088/0022-3700/14/21/016
Smith, P. L., & Kuehne, M. 1978, Royal Society of London Proceedings Series A, 362, 263, doi: 10.1098/rspa.1978.0133
Smith, W. W., & Gallagher, A. 1966, Physical Review, 145, 26, doi: 10.1103/PhysRev.145.26
Sobeck, J. S., Lawler, J. E., & Sneden, C. 2007, Astrophys. J., 667, 1267, doi: 10.1086/519987
Storey, P. J., & Zeippen, C. J. 2000, MNRAS, 312, 813, doi: 10.1046/j.1365-8711.2000.03184.x
Taylor, M. B. 2005, in Astronomical Society of the Pacific Conference Series, Vol. 347, Astronomical Data Analysis Software and Systems XIV, ed. P. Shopbell, M. Britton, & R. Ebert, 29
Teske, J. K., Khanal, S., & Ramírez, I. 2016, ApJ, 819, 19, doi: 10.3847/0004-637X/819/1/19
Theodosiou, C. E. 1989, Physical Review A, 39, 4880, doi: 10.1103/PhysRevA.39.4880
Ting, Y.-S., De Silva, G. M., Freeman, K. C., & Parker, S. J. 2012, MNRAS, 427, 882, doi: 10.1111/j.1365-2966.2012.22028.x
Ting, Y.-S., & Weinberg, D. H. 2021, arXiv e-prints, arXiv:2102.04992. https://arxiv.org/abs/2102.04992
Tokovinin, A. 2017, MNRAS, 468, 3461, doi: 10.1093/mnras/stx707
Tucci Maia, M., Meléndez, J., & Ramírez, I. 2014, ApJL, 790, L25, doi: 10.1088/2041-8205/790/2/L25
Vaeck, N., Godefroid, M., & Hansen, J. E. 1988, PhRvA, 38, 2830, doi: 10.1103/PhysRevA.38.2830
Virtanen, P., Gommers, R., Oliphant, T. E., et al. 2020, Nature Methods, 17, 261, doi: 10.1038/s41592-019-0686-2
Volz, U., Majerus, M., Liebel, H., Schmitt, A., & Schmoranzer, H. 1996, Physical Review Letters, 76, 2862, doi: 10.1103/PhysRevLett.76.2862
von der Goltz, D., Hansen, W., & Richter, J. 1984, PhyS, 30, 244, doi: 10.1088/0031-8949/30/4/005
Ward, L., Vogel, O., Arnesen, A., Hallin, R., & Wännström, A. 1985, PhyS, 31, 161, doi: 10.1088/0031-8949/31/3/001
Warner, B. 1968a, MNRAS, 140, 53
—. 1968b, MNRAS, 139, 115
Wenger, M., Ochsenbein, F., Egret, D., et al. 2000, A&AS, 143, 9, doi: 10.1051/aas:2000332
Werij, H. G. C., Greene, C. H., Theodosiou, C. E., & Gallagher, A. 1992, PhRvA, 46, 1248, doi: 10.1103/PhysRevA.46.1248
Whaling, W., & Brault, J. W. 1988, PhyS, 38, 707, doi: 10.1088/0031-8949/38/5/010
Whaling, W., Hannaford, P., Lowe, R. M., Biemont, E., & Grevesse, N. 1985, A&A, 153, 109
Wickliffe, M. E., & Lawler, J. E. 1997a, Journal of the Optical Society of America B Optical Physics, 14, 737, doi: 10.1364/JOSAB.14.000737
—. 1997b, ApJS, 110, 163, doi: 10.1086/312995
Wickliffe, M. E., Lawler, J. E., & Nave, G. 2000, J. Quant. Spectrosc. Radiat. Transfer, 66, 363, doi: 10.1016/S0022-4073(99)00173-9
Wickliffe, M. E., Salih, S., & Lawler, J. E. 1994, JQSRT, 51, 545, doi: 10.1016/0022-4073(94)90108-2
Wiese, W. L., & Martin, G. A. 1980, Wavelengths and transition probabilities for atoms and atomic ions: Part 2. Transition probabilities, ed. Reader, J., Corliss, C. H., Wiese, W. L., & Martin, G. A.

Wiese, W. L., Smith, M. W., & Glennon, B. M. 1966, Atomic transition probabilities. Vol.: Hydrogen through Neon. A critical data compilation, ed. Wiese, W. L., Smith, M. W., & Glennon, B. M. (US Government Printing Office)

Wiese, W. L., Smith, M. W., & Miles, B. M. 1969, Atomic transition probabilities. Vol. 2: Sodium through Calcium. A critical data compilation, ed. Wiese, W. L., Smith, M. W., & Miles, B. M. (US Government Printing Office)

Wolnik, S. J., Berthel, R. O., Larson, G. S., Carnevale, E. H., & Wares, G. W. 1968, Physics of Fluids, 11, 1002, doi: 10.1063/1.1692033

Wolnik, S. J., Berthel, R. O., & Wares, G. W. 1970, ApJ, 162, 1037, doi: 10.1086/150735

—. 1971, ApJL, 166, L31+, doi: 10.1086/180733

Wood, M. P., Lawler, J. E., Sneden, C., & Cowan, J. J. 2013a, ApJS, 208, 27, doi: 10.1088/0067-0049/208/2/27

—. 2013b, ApJS, 208, 27, doi: 10.1088/0067-0049/208/2/27

—. 2014, ApJS, 211, 20, doi: 10.1088/0067-0049/211/2/20

Xu, H., Jiang, Z., Zhang, Z., et al. 2003a, Journal of Physics B Atomic Molecular Physics, 36, 1771

Xu, H. L., Svanberg, S., Cowan, R. D., et al. 2003b, Monthly Notices Roy. Astron. Soc., 346, 433, doi: 10.1046/j.1365-2966.2003.07107.x

Xu, H. L., Svanberg, S., Quinet, P., Garnir, H. P., & Biémont, E. 2003c, Journal of Physics B Atomic Molecular Physics, 36, 4773, doi: 10.1088/0953-4075/36/24/002

Yan, Z.-C., Tambasco, M., & Drake, G. W. F. 1998, PhRvA, 57, 1652, doi: 10.1103/PhysRevA.57.1652

Zatsarinny, O., & Bartschat, K. 2006, Journal of Physics B Atomic Molecular Physics, 39, 2861, doi: 10.1088/0953-4075/39/12/019

Zhao, J. K., Oswalt, T. D., Willson, L. A., Wang, Q., & Zhao, G. 2012, ApJ, 746, 144, doi: 10.1088/0004-637X/746/2/144

Zhiguo, Z., Li, Z. S., Lundberg, H., et al. 2000, Journal of Physics B Atomic Molecular Physics, 33, 521, doi: 10.1088/0953-4075/33/3/319

Zhiguo, Z., Zhongshan, L., & Zhankui, J. 1999, European Physical Journal D, 7, 499, doi: 10.1007/s100530050377